Conventional finite elements *versus* MITC in structural analysis of moderately thick plates

Rui Rodrigues Araújo

October 29, 2013

Abstract

In the present work, the theory of Reissner-Mindlin plates is developed for the static, free vibration and linear stability cases. By applying Hamilton's principle it is possible to derive the equilibrium equations in the domain and on the static boundary of the problem and compatibility equations on the kinematic boundary.

Among the several existing numerical methods, the Finite Element Method (FEM) has proved the most adequate to obtain approximated solutions in structural analysis. It is essential to be aware of the errors involved in the approximation of the solution, which depend on the type of element and its characteristic dimension, in order to decide which type of element is the most appropriate to the case under consideration. Thus, in the FEM context, this dissertation sought to analyze and compare the results obtained using two types of finite elements with different formulations: the conventional elements, whose formulation is based on an approximation of the generalized displacement field, and the MITC elements, based on mixed formulation in convective coordinates.

Here Were considered the conventional quadrilateral elements, Lagrangian (QL4, QL9, QL16, QL25, QL36) and Serendipity (QS8, QS12, QS16, QS20), and triangular (T3, T6, T10, T15, T21), and plate (MITC4, MITC9p, MITC16p, MITC7p and MITC12p) and shell (MITC9s and MITC16s) MITC elements. A description of each element is made, besides a discussion about some aspects in the formulation of each element type (conventional and MITC). Its implementation, made in MATLAB environment, allowed to obtain important information about the quality of the elements.

To evaluate the behavior and performance of the several finite elements under consideration for static, free vibration and linear stability analysis, various tests of a simply supported rectangular plate, whose exact solution can be found in the relevant literature, were made: (i) determination of the strain energy convergence and the sensitivity to shear-locking phenomenon of a plate with uniformly distributed load, (ii) assess the convergence of the natural vibration frequencies and (iii) calculate the convergence of loading parameters of instability for a plate subjected to bi-axial compression. From their results, conclusions are drawn about the advantages and disadvantages inherent to each type of element, taking into account the approximation errors.

Keywords: Finite Element Method, thick plates, MITC, *shear-locking*, conventional elements.

1 Theory of Reissner-Mindlin plates

Consider a body, V, with the particular shape. Its geometry can be described by,

$$V = \left\{ (x_1, x_2, x_3) \in \mathbb{R}^3 | (x_1, x_2) \in \Omega \subset \mathbb{R}^2, x_3 \in \left[-\frac{h}{2}, \frac{h}{2} \right] \right\}$$

where h is the *thickness* of the plate and Ω denotes the *middle plane*, whose *contour* its identified by Γ. The boundary of Ω, Γ, can be decomposed into the kinematic, Γ_u, and static, Γ_t, parts, where $\Gamma = \overline{\Gamma_t \cup \Gamma_u}$, $\Gamma_t \cap \Gamma_u = \emptyset$ and $\overline{\Omega} = \Omega \cup \Gamma$.

The relation between the continuum displacements and their generalized analogous is assumed to be given by

$$u_\alpha(x_1, x_2, x_3) = x_3 \, \theta_\alpha(x_1, x_2) \tag{1a}$$

$$u_3(x_1, x_2, x_3) = w(x_1, x_2) \tag{1b}$$

where θ_α is the *rotation vector* components and w is the *transverse displacement* field.

The generalized *compatibility equations* in the domain are given by,

$$\chi_{\alpha\beta} = \frac{1}{2} \left(\theta_{\alpha,\beta} + \theta_{\beta,\alpha} + x_3^2 \theta_{\gamma,\alpha} \theta_{\gamma,\beta} + w_{,\alpha} \, w_{,\beta} \right) \tag{2a}$$

$$\gamma_\alpha = w_{,\alpha} + \theta_\alpha \tag{2b}$$

where $\chi_{\alpha\beta}$ are the *curvature tensor* components and γ_α are the middle plane *distortion vector* components. The two last terms of the second member of (2a) represent some nonlinear components, introduced in order to perform linear stability analysis.

The generalized compatibility equations on the kinematic

part of the boundary, Γ_u, are:

$$w - \overline{w} = 0 \tag{3a}$$
$$\theta_\alpha - \overline{\theta}_\alpha = 0 \tag{3b}$$

The generalized *equilibrium equations* in the domain are,

$$m_{\alpha\beta,\beta} - v_\alpha + \left(\frac{h^3}{12}\,\sigma_{\gamma\beta}\,\theta_{\alpha,\beta}\right)_{,\gamma} + \overline{m}_\alpha - \theta_\alpha\,k_w^\theta\,\frac{h^3}{12} = I_2\,\ddot{\theta}_\alpha \tag{4a}$$
$$v_{\alpha,\alpha} + (h\,\sigma_{\alpha\beta}\,w_{,\beta})_{,\alpha} + \overline{p} - w\,k_w^w\,h = I_0\,\ddot{w} \tag{4b}$$

where $m_{\alpha\beta}$ are the *moment tensor* components, v_α are the *shear force vector* components, $\sigma_{\gamma\beta}$ are the *in-plane* or *membrane (Cauchy) stress tensor* components, $\overline{m}_\alpha$ are the *applied moment in the domain vector* components, $\overline{p}$ is the *applied load in the domain*, k_w^θ and k_w^w are the *rotational and translational Winkler foundation modulus*, $\ddot{\theta}_\alpha$ are the *angular acceleration vector* components, $\ddot{w}$ is the middle plane *acceleration* and,

$$I_\alpha = \int_{-\frac{h}{2}}^{\frac{h}{2}} \rho\,x_3^\alpha\,\mathrm{d}x_3 \tag{5}$$

is the α order Inertia moment. The shear force vector and the moment tensor components are defined as:

$$v_\alpha = \int_{-\frac{h}{2}}^{\frac{h}{2}} \sigma_{\alpha 3}\,\mathrm{d}x_3 \tag{6a}$$
$$m_{\alpha\beta} = \int_{-\frac{h}{2}}^{\frac{h}{2}} x_3\,\sigma_{\alpha\beta}\,\mathrm{d}x_3 \tag{6b}$$

Consider that *body forces*, $\overline{b}_i$, and *surface tractions*, $\overline{t}_i$, act in the domain, Ω, and on the static boundary, Γ_t. Therefore, the applied load and moments in the domain are

$$\overline{p} = \int_{-\frac{h}{2}}^{\frac{h}{2}} \overline{b}_3\,\mathrm{d}x_3 + \overline{t}_3\big|_{x_3=\frac{h}{2}} + \overline{t}_3\big|_{x_3=-\frac{h}{2}} \tag{7a}$$
$$\overline{m}_\alpha = \int_{-\frac{h}{2}}^{\frac{h}{2}} x_3\,\overline{b}_\alpha\,\mathrm{d}x_3 + \left[\frac{h}{2}\,\overline{t}_\alpha\right]\Big|_{x_3=\frac{h}{2}} + \left[-\frac{h}{2}\,\overline{t}_\alpha\right]\Big|_{x_3=-\frac{h}{2}} \tag{7b}$$

The generalized *equilibrium equations* on the static boundary, Γ_t, are,

$$m_{\alpha\beta}\,n_\beta + \frac{h^3}{12}\,\sigma_{\gamma\beta}\,\theta_{\alpha,\beta}\,n_\gamma + \overline{m}_\alpha^\Gamma = 0 \tag{8a}$$
$$v_\alpha\,n_\alpha + h\,\sigma_{\alpha\beta}\,w_{,\beta}\,n_\alpha + \overline{p}^\Gamma = 0 \tag{8b}$$

where n_β are the *unit outward normal vector* components, $\overline{m}_\alpha^\Gamma$ are the *applied moment on the boundary vector* components and $\overline{p}^\Gamma$ is the *applied load on the boundary*.

The static boundary counterparts of (7) are

$$\overline{p}^\Gamma = \int_{-\frac{h}{2}}^{\frac{h}{2}} \overline{t}_3\,\mathrm{d}x_3, \tag{9a}$$
$$\overline{m}_\alpha^\Gamma = \int_{-\frac{h}{2}}^{\frac{h}{2}} x_3\,\overline{t}_\alpha\,\mathrm{d}x_3. \tag{9b}$$

The generalized *constitutive relation* between moments and curvatures can be written as

$$m_{\alpha\beta} = C_{\alpha\beta\gamma\delta}\,\chi_{\gamma\delta} \tag{10}$$

where $C_{\alpha\beta\gamma\delta}$ are the (fourth order) *constitutive tensor* components. For homogeneous and isotropic material this tensor renders

$$C_{\alpha\beta\gamma\delta} = D_f\,\left(\frac{1-\nu}{2}\,(\delta_{\alpha\gamma}\,\delta_{\beta\delta} + \delta_{\alpha\delta}\,\delta_{\beta\gamma}) + \nu\,\delta_{\alpha\beta}\,\delta_{\delta\gamma}\right) \tag{11}$$

where $D_f = \frac{E\,h^3}{12(1-\nu^2)}$ is the *bending stiffness*. Here E is the *elasticity modulus* and ν is the *Poisson's ratio*. The counterpart of (10), relating the shear forces and the distortions, is given by

$$v_\alpha = D_s\,\gamma_\alpha \tag{12}$$

where $D_s = \kappa\,G\,h$ is the shear rigidity, being κ the usual shear factor correction term ($\kappa = \frac{5}{6}$) and $G = \frac{E}{2(1+\nu)}$ is the *shear modulus*.

2 The weak form

Since it is intended to include free-vibration analysis in the present work, the weak form will be derived from the Hamilton's principle. For the moderately thick plate case, this can be written as

$$\begin{aligned}\int_\Omega (m_{\alpha\beta}\,\delta\chi_{\alpha\beta} + v_\alpha\,\gamma_{\alpha 3})\,\mathrm{d}\Omega + \int_\Omega \Big(\theta_{\gamma,\alpha}\,\frac{h^3}{12}\,\sigma_{\alpha\beta}\,\delta\theta_{\gamma,\alpha} \\ + w_{,\beta}\,h\,\sigma_{\alpha\beta}\delta\theta_{\gamma,\alpha})\,\mathrm{d}\Omega + \int_\Omega \left(\theta_\alpha\frac{h^3}{12}k_w^\theta\,\delta\theta_\alpha + w\,h\,k_w^w\delta w\right)\mathrm{d}\Omega \\ + \int_\Omega \left(\ddot{\theta}_\alpha\,I_2\,\delta\theta_\alpha + \ddot{w}\,I_0\,\delta w\right)\mathrm{d}\Omega - \int_\Omega (\overline{m}_\alpha\delta\theta_\alpha + \overline{p}_\alpha\delta w)\,\mathrm{d}\Omega \\ - \int_\Gamma \left(\overline{m}_\alpha^\Gamma\delta\theta_\alpha + \overline{p}_\alpha^\Gamma\delta w\right)\mathrm{d}\Gamma = 0.\end{aligned} \tag{13}$$

The first three terms represent the *total strain energy* variation, which follow from the (i) moment and shear effects and is linear in the generalized displacements, (ii) the in-plane stresses, which is nonlinear in the generalized displacements and (iii) the Winkler foundation. The fourth term is the *kinetic energy of the moving body* variation. The fifth and sixth terms are the *potential energy of the loading* variation from the domain and static boundary, respectively.

3 The Finite Element discretization

3.1 FEM equation

Consider a generic element (e). The generalized displacement field of this element can be written as

$$\mathbf{u}^{(e)} = \mathbf{\Psi}^{(e)}\,\mathbf{d}^{(e)} \tag{14}$$

where $\mathbf{\Psi}^{(e)}$ gathers the *element approximation functions* and $\mathbf{d}^{(e)}$ are the associated *generalized nodal displacements*, *i.e.*,

$$\mathbf{\Psi}^{(e)} = \begin{bmatrix} \mathbf{\Psi}^{w(e)} & \mathbf{O} & \mathbf{O} \\ \mathbf{O} & \mathbf{\Psi}^{\theta(e)} & \mathbf{O} \\ \mathbf{O} & \mathbf{O} & \mathbf{\Psi}^{\theta(e)} \end{bmatrix}, \quad \mathbf{d}^{(e)} = \begin{Bmatrix} \widehat{\boldsymbol{w}}^{(e)} \\ \widehat{\boldsymbol{\theta}}_1^{(e)} \\ \widehat{\boldsymbol{\theta}}_2^{(e)} \end{Bmatrix} \tag{15}$$

Hence, the variations and the acceleration of the generalized displacement field are, respectively,

$$\delta\mathbf{u}^{(e)} = \mathbf{\Psi}^{(e)}\,\delta\mathbf{d}^{(e)} \tag{16a}$$

$$\ddot{\mathbf{u}}^{(e)} = \mathbf{\Psi}^{(e)}\,\ddot{\mathbf{d}}^{(e)} \tag{16b}$$

By substituting the approximations (14) and (16) into the weak form (13) it is obtained the elementar nodal equilibrium equations

$$\left(\mathbf{K}_p^{(e)} - \lambda\,\mathbf{G}^{(e)} + \mathbf{K}_w^{(e)}\right)\mathbf{d}^{(e)} + \mathbf{M}^{(e)}\,\ddot{\mathbf{d}}^{(e)} = \mathbf{f}^{(e)}, \quad \forall\,\delta\mathbf{d}^{(e)}\,. \tag{17}$$

The several quantities present in the previous system are detailed in the following.

The plate stiffness was decomposed into the flexural and shear parts

$$\mathbf{K}_p^{(e)} = \mathbf{K}_{ff}^{(e)} + \mathbf{K}_{ss}^{(e)}, \tag{18}$$

where

$$\mathbf{K}_{ff}^{(e)} = \int_{\Omega^{(e)}} \mathbf{B}_f^{(e)T}\,\mathbf{D}_f^{(e)}\,\mathbf{B}_f^{(e)}\,\mathrm{d}\Omega^{(e)} \tag{19a}$$

$$\mathbf{K}_{ss}^{(e)} = \int_{\Omega^{(e)}} \mathbf{B}_s^{(e)T}\,\mathbf{D}_s^{(e)}\,\mathbf{B}_s^{(e)}\,\mathrm{d}\Omega^{(e)}, \tag{19b}$$

being the matrices $\mathbf{B}_f^{(e)}$ and $\mathbf{B}_s^{(e)}$ given by

$$\mathbf{B}_f^{(e)} = \boldsymbol{\partial}_f\,\mathbf{\Psi}^{(e)}, \quad \mathbf{B}_s^{(e)} = \boldsymbol{\partial}_s\,\mathbf{\Psi}^{(e)}. \tag{20}$$

$\boldsymbol{\partial}_f$ and $\boldsymbol{\partial}_s$ are the differential operators associated with the flexure and shear, respectively, defined by

$$\boldsymbol{\partial}_f = \begin{bmatrix} 0 & \partial_1 & 0 \\ 0 & 0 & \partial_2 \\ 0 & \partial_2 & \partial_1 \end{bmatrix} \quad \text{and} \quad \boldsymbol{\partial}_s = \begin{bmatrix} \partial_1 & 1 & 0 \\ \partial_2 & 0 & 1 \end{bmatrix}. \tag{21}$$

The constitutive matrices are

$$\mathbf{D}_f = D_f \begin{bmatrix} 1 & \nu & 0 \\ \nu & 1 & 0 \\ 0 & 0 & \frac{(1-\nu)}{2} \end{bmatrix}, \quad \mathbf{D}_s = D_s \begin{bmatrix} 1 & 0 \\ 0 & 1 \end{bmatrix}. \tag{22}$$

It is convenient to impose that the membrane stress tensor, $\boldsymbol{\sigma}$, depends linearly on a load parameter, λ. Hence $\boldsymbol{\sigma} = -\lambda\boldsymbol{\sigma}_0$, where $\boldsymbol{\sigma}_0$ is a reference membrane stress tensor. Let

$$\boldsymbol{\sigma}_0 = \begin{bmatrix} \sigma_{11}^0 & \sigma_{12}^0 \\ \sigma_{21}^0 & \sigma_{22}^0 \end{bmatrix}, \quad \mathbf{L} = \begin{bmatrix} \partial_1 & 0 & 0 \\ \partial_2 & 0 & 0 \\ 0 & \partial_1 & 0 \\ 0 & \partial_2 & 0 \\ 0 & 0 & \partial_1 \\ 0 & 0 & \partial_2 \end{bmatrix} \quad \text{and} \tag{23a}$$

$$\boldsymbol{\tau}_0 = \begin{bmatrix} h\,\boldsymbol{\sigma}_0 & \mathbf{O} & \mathbf{O} \\ \mathbf{O} & \frac{h^3}{12}\,\boldsymbol{\sigma}_0 & \mathbf{O} \\ \mathbf{O} & \mathbf{O} & \frac{h^3}{12}\,\boldsymbol{\sigma}_0 \end{bmatrix}. \tag{23b}$$

Then, the geometric contribution to the plate stiffness is given by

$$\mathbf{G}^{(e)} = \int_\Omega (\mathbf{L}\,\mathbf{\Psi}^{(e)T})\,\boldsymbol{\tau}_0\,(\mathbf{L}\,\mathbf{\Psi}^{(e)})\,\mathrm{d}\Omega. \tag{24}$$

The Winkler type of foundation adds the following term to the plate stiffness

$$\mathbf{K}_w^{(e)} = \int_\Omega \mathbf{\Psi}^{(e)T}\,\widetilde{\mathbf{K}}_w^{(e)}\,\mathbf{\Psi}^{(e)}\,\mathrm{d}\Omega, \tag{25}$$

where

$$\widetilde{\mathbf{K}}_w = \begin{bmatrix} h\,k_w^w & 0 & 0 \\ 0 & \frac{h^3}{12}\,k_w^\theta & 0 \\ 0 & 0 & \frac{h^3}{12}\,k_w^\theta \end{bmatrix}. \tag{26}$$

The mass matrix is expressed by

$$\mathbf{M}^{(e)} = \int_\Omega \mathbf{\Psi}^{(e)T}\,\boldsymbol{\rho}\,\mathbf{\Psi}^{(e)}\,\mathrm{d}\Omega \tag{27}$$

where

$$\boldsymbol{\rho} = \begin{bmatrix} I_0 & \mathbf{0} & \mathbf{0} \\ \mathbf{0} & I_2 & \mathbf{0} \\ \mathbf{0} & \mathbf{0} & I_2 \end{bmatrix} \tag{28}$$

is a generalized density matrix.

Finally, the equivalent nodal load vector is given by

$$\mathbf{f}^{(e)} = \mathbf{f}^{(e)\Omega} + \mathbf{f}^{(e)\Gamma} \tag{29}$$

where

$$\mathbf{f}^{(e)\Omega} = \int_{\Omega^{(e)}} \mathbf{\Psi}^{(e)T}\,\overline{\mathbf{b}}^{(e)}\,\mathrm{d}\Omega^{(e)}, \quad \mathbf{f}^{(e)\Gamma} = \int_{\Gamma^{(e)}} \mathbf{\Psi}^{(e)T}\,\overline{\mathbf{t}}\,\mathrm{d}\Gamma_t^{(e)}, \tag{30}$$

and

$$\overline{\mathbf{b}} = \begin{Bmatrix} \overline{p} \\ \overline{m}_1 \\ \overline{m}_2 \end{Bmatrix}, \quad \overline{\mathbf{t}} = \begin{Bmatrix} \overline{p}^\Gamma \\ \overline{m}_1^\Gamma \\ \overline{m}_2^\Gamma \end{Bmatrix}. \tag{31}$$

The global equation system is obtained using the standard assembly scheme, *i.e.*,

$$\mathbf{K}_p = \mathop{\mathsf{A}}_{e=1}^{n_e} \mathbf{K}_p^{(e)} \tag{32a}$$

$$\mathbf{f} = \mathop{\mathsf{A}}_{e=1}^{n_e} \mathbf{f}^{(e)}, \tag{32b}$$

The global system is then given by

$$(\mathbf{K}_p - \lambda\,\mathbf{G} + \mathbf{K}_w)\,\mathbf{d} + \mathbf{M}\,\ddot{\mathbf{d}} = \mathbf{f}, \quad \forall\,\delta\mathbf{d}\,. \tag{33}$$

Kinematic boundary conditions are imposed by the usual splitting in free and constrained degrees of freedom.

3.2 Static analysis

For the static analysis analysis case, we have

$$\ddot{\mathbf{d}} = \mathbf{0}, \quad \lambda = 0. \tag{34}$$

Hence, the FEM equation in (33), becomes

$$(\mathbf{K}_p + \mathbf{K}_w)\,\mathbf{d} = \mathbf{f}\,. \tag{35}$$

Defining, $\mathbf{K}^{(e)}$, as

$$\mathbf{K}^{(e)} = \mathbf{K}_p^{(e)} + \mathbf{K}_w^{(e)}\,, \tag{36}$$

after the assembly process, the equation (35) becomes the classic FEM equation

$$\mathbf{K}\,\mathbf{d} = \mathbf{f}\,, \tag{37}$$

3.3 Free-vibration analysis

In the Free-vibration problem, we have

$$\mathbf{f} = \mathbf{0}, \quad \lambda = 0\,. \tag{38}$$

Thus, the FEM equation (33), results in

$$(\mathbf{K}_p + \mathbf{K}_w)\,\mathbf{d} + \mathbf{M}\,\ddot{\mathbf{d}} = \mathbf{0}\,. \tag{39}$$

Considering (36), the previous equation is given by

$$\mathbf{K}\,\mathbf{d} + \mathbf{M}\,\ddot{\mathbf{d}} = \mathbf{0}\,. \tag{40}$$

By introducing a convenient separation of time and space variables, the following eigenvalue problem is obtained

$$|\mathbf{K} - \omega^2\,\mathbf{M}| = 0\,, \tag{41}$$

from which it is found the *vibration frequencies*, w_n, of the plate. The configuration of each mode can be obtained by determining the eigenvector corresponding to each eigenvalue.

3.4 Linear stability analysis

In the linear stability analysis, we have

$$\ddot{\mathbf{d}} = \mathbf{0}\,, \quad \mathbf{f} = \mathbf{0}\,. \tag{42}$$

Therefore, the FEM equation (33), results in

$$(\mathbf{K}_p + \mathbf{K}_w)\;\mathbf{d} - \lambda\,\mathbf{G}\,\mathbf{d} = \mathbf{0} \quad \Leftrightarrow \quad (\mathbf{K} - \lambda\,\mathbf{G})\,\mathbf{d} = \mathbf{0}\,. \tag{43}$$

As in the vibration analysis, it is possible to show that — after discretization — the following eigenvalue problem is obtained

$$|\mathbf{K} - \lambda\,\mathbf{G}| = 0\,. \tag{44}$$

The eigenvalues of the problem represent the *load parameters of the membrane critical stresses*, λ_n.

4 A mixed element formulation in convective coordinates

4.1 Element formulation in convective coordinates

Consider a generic finite element — triangular or quadrilateral — whose geometry is defined parametrically by

$$\boldsymbol{x} = x_\alpha\;(\boldsymbol{\xi})\;\mathbf{e}_\alpha + x_3\;(\zeta)\;\mathbf{e}_3\,, \tag{45}$$

where $x_\alpha\,(\boldsymbol{\xi}) = \sum_{i=1}^{n} \psi_i\,(\boldsymbol{\xi})\;x_{\alpha i}$ and $x_3\,(\zeta) = \zeta$. n is the number of nodes used to represent the geometry of the element, $x_{\alpha i}$ corresponds to the coordinate in the α direction at node i, $\widehat{\Omega}$ represents the domain of the master-element and $\zeta \in \left[-\frac{h}{2}, -\frac{h}{2}\right]$.

The displacement field for these elements is given by

$$\mathbf{u} = x_3\,\theta_\alpha\;(\boldsymbol{\xi})\;\mathbf{e}_\alpha + w\;(\boldsymbol{\xi})\;\mathbf{e}_3\,, \tag{46}$$

where

$$\theta_\alpha\,(\boldsymbol{\xi}) = \sum_{i=1}^{p} \psi_i^\theta\;(\boldsymbol{\xi})\;\theta_{\alpha i} = \boldsymbol{\Psi}^\theta\,(\boldsymbol{\xi})\;\widehat{\boldsymbol{\theta}}_\alpha \tag{47a}$$

$$w\;(\boldsymbol{\xi}) = \sum_{i=1}^{q} \psi_i^w\;(\boldsymbol{\xi})\;w_i = \boldsymbol{\Psi}^w\,(\boldsymbol{\xi})\;\widehat{\boldsymbol{w}}\,. \tag{47b}$$

p is the number of nodes of the element with free rotation degrees of freedom, θ_α, and q is the number of nodes of the element with free transversal displacements degrees of freedom , w.

For the mixed formulation of MITC elements, it's necessary to evaluate the covariant components of the distortion from $\mathbf{u}$ at certain points, called *tying points* or at integration points. To this end, the components of the strain tensor in covariant coordinates are calculated by means of

$$\widetilde{\varepsilon}_{ij} = \frac{1}{2}\left((\boldsymbol{x} + \mathbf{u})_{,i} \cdot (\boldsymbol{x} + \mathbf{u})_{,j} - \boldsymbol{x}_{,i} \cdot \boldsymbol{x}_{,j}\right)\,. \tag{48}$$

Regarding that $\boldsymbol{\gamma}$ can be written in a contravariant base, $\mathbf{g}^\alpha$, by $\boldsymbol{\gamma} = \widetilde{\gamma}_\alpha\,\mathbf{g}^\alpha$, and neglecting nonlinear terms, the covariant components are given by

$$\widetilde{\gamma}_\alpha = 2\widetilde{\varepsilon}_{\alpha 3} = \boldsymbol{x}_{,\alpha} \cdot \mathbf{u}_{,3} + \boldsymbol{x}_{,3} \cdot \mathbf{u}_{,\alpha}\,. \tag{49}$$

Performing the expansion of the above expression, we have, in matrix notation,

$$\begin{Bmatrix} \widetilde{\gamma}_1 \\ \widetilde{\gamma}_2 \end{Bmatrix} = \begin{bmatrix} \partial_1 & x_{1,1} & x_{2,1} \\ \partial_2 & x_{1,2} & x_{2,2} \end{bmatrix} \begin{Bmatrix} w \\ \theta_1 \\ \theta_2 \end{Bmatrix}\,, \tag{50}$$

with $\partial_\alpha = \frac{\partial}{\partial \xi_\alpha}$. Realizing that the Jacobian matrix is

$$\mathbf{J} = \begin{bmatrix} x_{1,1} & x_{1,2} \\ x_{2,1} & x_{2,2} \end{bmatrix} \tag{51}$$

and having in consideration that

$$x_{1,\alpha}\,\frac{\partial(.)}{\partial x_1}+x_{2,\alpha}\,\frac{\partial(.)}{\partial x_2}=\frac{\partial(.)}{\partial x_1}\,\frac{\partial x_1}{\partial \xi_\alpha}+\frac{\partial(.)}{\partial x_2}\,\frac{\partial x_2}{\partial \xi_\alpha}=\frac{\partial(.)}{\partial \xi_\alpha}=\partial_\alpha(.)\,, \tag{52}$$

the expression (50) comes down to

$$\begin{Bmatrix}\widetilde{\gamma}_1\\ \widetilde{\gamma}_2\end{Bmatrix}=\begin{bmatrix}x_{1,1} & x_{2,1}\\ x_{1,2} & x_{2,2}\end{bmatrix}\begin{bmatrix}\frac{\partial}{\partial x_1} & 1 & 0\\ \frac{\partial}{\partial x_2} & 0 & 1\end{bmatrix}\begin{Bmatrix}w\\ \theta_1\\ \theta_2\end{Bmatrix}=\mathbf{J}^T\,\boldsymbol{\partial}_s\,\mathbf{u}\,, \tag{53}$$

where $\boldsymbol{\partial}_s$ is given in (21). At last, defining $\widetilde{\boldsymbol{\partial}}_s=\mathbf{J}^T\,\boldsymbol{\partial}_s$, we are left with

$$\widetilde{\boldsymbol{\gamma}}=\widetilde{\boldsymbol{\partial}}_s\,\mathbf{u}\,, \tag{54}$$

being

$$\widetilde{\boldsymbol{\partial}}_s=\begin{bmatrix}\partial_1 & x_{1,1} & x_{2,1}\\ \partial_2 & x_{1,2} & x_{2,2}\end{bmatrix}. \tag{55}$$

4.2 Mixed formulation u-$\underset{\sim}{\lambda}$-$\widetilde{\gamma}$

Consider the modified functional of total potential energy, where (only) the compatibility equation, $\boldsymbol{\gamma}=\boldsymbol{\partial}_s\mathbf{u}$, is relaxed, and it's weak imposition is made by Lagrange multipliers,

$$\begin{aligned}\overline{\Pi}(\mathbf{u},\boldsymbol{\lambda},\boldsymbol{\gamma})=\Pi(\mathbf{u})&-\int_\Omega \boldsymbol{\lambda}^{\Omega T}(\boldsymbol{\gamma}-\boldsymbol{\gamma}^{DI})\,\mathrm{d}\Omega\\ &-\sum_{i=1}^{n}\widehat{\lambda}_i^{\Gamma}\,\left[(\boldsymbol{\gamma}-\boldsymbol{\gamma}^{DI})\cdot\mathbf{t}\right]\big|_{\boldsymbol{\xi}=\boldsymbol{\xi}_i}\,,\end{aligned} \tag{56}$$

where it is imposed locally that $\chi=\boldsymbol{\partial}_f\mathbf{u}$, $\boldsymbol{\sigma}=\mathbf{D}\boldsymbol{\varepsilon}$, $\boldsymbol{\gamma}^{DI}=\boldsymbol{\partial}_s\,\mathbf{u}$, and n is the number of points where it's required that the projection of the average distortion in the direction of the tangential vector to the boundary, $\mathbf{t}$, is zero, *i.e.*, where $(\boldsymbol{\gamma}-\boldsymbol{\gamma}^{DI})\cdot\mathbf{t}=0$, and $\boldsymbol{\xi}_i$ are the coordinates of *tying points* on the boundary of the element. Hence, $\Pi(\mathbf{u},\gamma)$ is given by

$$\begin{aligned}\Pi(\mathbf{u},\gamma)=\frac{1}{2}\int_\Omega(\boldsymbol{\partial}_f\,\mathbf{u})^T\,\mathbf{D}_f\,(\boldsymbol{\partial}_f\,\mathbf{u})\,\mathrm{d}\Omega+\frac{1}{2}\int_\Omega\boldsymbol{\gamma}^T\,\mathbf{D}_s\,\boldsymbol{\gamma}\,\mathrm{d}\Omega\\ -\int_\Omega\mathbf{u}^T\,\overline{\mathbf{b}}\,\mathrm{d}\Omega-\int_\Gamma\mathbf{u}^T\,\overline{\mathbf{t}}\,\mathrm{d}\Gamma\,.\end{aligned} \tag{57}$$

The above form is not suitable for the MITC elements, because it is not in terms of convective coordinates. Thus, it's necessary to rewrite each of the terms involving $\boldsymbol{\gamma}$ and $\boldsymbol{\lambda}$:

$$\boldsymbol{\gamma}=\gamma_\alpha\,\mathbf{e}_\alpha=\widetilde{\gamma}_\alpha\,\mathbf{g}^\alpha \tag{58a}$$

$$\boldsymbol{\gamma}^{DI}=\gamma_\alpha^{DI}\,\mathbf{e}_\alpha=\widetilde{\gamma}_\alpha^{DI}\,\mathbf{g}^\alpha \tag{58b}$$

$$\boldsymbol{\lambda}^{\Omega}=\lambda_\alpha^{\Omega}\,\mathbf{e}_\alpha=\widetilde{\lambda}^{\Omega\,\alpha}\,\mathbf{g}_\alpha \tag{58c}$$

$$\widehat{\lambda}_i^{\Gamma}=\underset{\sim}{\widehat{\lambda}}_i^{\Gamma}\,, \tag{58d}$$

Note that $\widetilde{\boldsymbol{\gamma}}^{DI}=\widetilde{\boldsymbol{\partial}}_s\,\mathbf{u}=\mathbf{J}^T\,\boldsymbol{\partial}_s\,\mathbf{u}$.

The covariant and contravariant base vectors are obtained, respectively, from

$$\left[\mathbf{g}^1\,\mathbf{g}^2\right]=\left[\;\boldsymbol{x}_{,1}\;\middle|\;\boldsymbol{x}_{,2}\;\right]=\mathbf{J} \tag{59a}$$

$$\left[\mathbf{g}^1\,\mathbf{g}^2\right]=\left(\mathbf{J}^T\,\mathbf{J}\right)^{-T}\,\left[\mathbf{g}_1\,\mathbf{g}_2\right]=\left(\mathbf{J}^T\,\mathbf{J}\right)^{-T}\,\mathbf{J}\,. \tag{59b}$$

Consider now the elementary approximations[1]

$$\mathbf{u}=\boldsymbol{\Psi}^u\,\widehat{\mathbf{u}} \tag{60a}$$

$$\widetilde{\boldsymbol{\gamma}}=\boldsymbol{\Psi}^{\widetilde{\gamma}}\,\widehat{\widetilde{\boldsymbol{\gamma}}} \tag{60b}$$

$$\underset{\sim}{\boldsymbol{\lambda}}^{\Omega}=\boldsymbol{\Psi}^{\underset{\sim}{\lambda}}\,\underset{\sim}{\widehat{\boldsymbol{\lambda}}}^{\Omega}\,. \tag{60c}$$

Setting

$$\boldsymbol{\Upsilon}=\begin{Bmatrix}\left[\mathbf{t}^T\,\boldsymbol{\Psi}^{\widetilde{\gamma}}\right]\big|_{\boldsymbol{\xi}=\boldsymbol{\xi}_1}\\ \left[\mathbf{t}^T\,\boldsymbol{\Psi}^{\widetilde{\gamma}}\right]\big|_{\boldsymbol{\xi}=\boldsymbol{\xi}_2}\\ \vdots\\ \left[\mathbf{t}^T\,\boldsymbol{\Psi}^{\widetilde{\gamma}}\right]\big|_{\boldsymbol{\xi}=\boldsymbol{\xi}_n}\end{Bmatrix},\quad \boldsymbol{\Lambda}=\begin{Bmatrix}\left[\mathbf{t}^T\,\widetilde{\boldsymbol{\partial}}_s\,\boldsymbol{\Psi}^{u}\right]\big|_{\boldsymbol{\xi}=\boldsymbol{\xi}_1}\\ \left[\mathbf{t}^T\,\widetilde{\boldsymbol{\partial}}_s\,\boldsymbol{\Psi}^{u}\right]\big|_{\boldsymbol{\xi}=\boldsymbol{\xi}_2}\\ \vdots\\ \left[\mathbf{t}^T\,\widetilde{\boldsymbol{\partial}}_s\,\boldsymbol{\Psi}^{u}\right]\big|_{\boldsymbol{\xi}=\boldsymbol{\xi}_n}\end{Bmatrix}, \tag{61a}$$

$$\mathbf{K}_{ff}=\int_\Omega\mathbf{B}_f^T\mathbf{D}_f\mathbf{B}_f\,\mathrm{d}\Omega, \tag{61b}$$

$$\mathbf{K}_{\widetilde{\gamma}\widetilde{\gamma}}=\int_\Omega\left(\left[\mathbf{g}^1\,\mathbf{g}^2\right]\,\boldsymbol{\Psi}^{\widetilde{\gamma}}\right)^T\,\mathbf{D}_s\,\left(\left[\mathbf{g}^1\,\mathbf{g}^2\right]\,\boldsymbol{\Psi}^{\widetilde{\gamma}}\right)\,\mathrm{d}\Omega, \tag{61c}$$

$$\mathbf{K}_{s\underset{\sim}{\lambda}}=\mathrm{diag}\left(\int_\Omega\left(\widetilde{\boldsymbol{\partial}}_s\,\boldsymbol{\Psi}^u\right)^T\,\boldsymbol{\Psi}^{\underset{\sim}{\lambda}}\,\mathrm{d}\Omega,\,\boldsymbol{\Lambda}\right), \tag{61d}$$

$$\mathbf{K}_{\widetilde{\gamma}\underset{\sim}{\lambda}}=\mathrm{diag}\left(\int_\Omega\boldsymbol{\Psi}^{\widetilde{\gamma}T}\boldsymbol{\Psi}^{\underset{\sim}{\lambda}}\,\mathrm{d}\Omega,\,\boldsymbol{\Upsilon}\right) \tag{61e}$$

$$\mathbf{K}_{\underset{\sim}{\lambda}s}=\mathbf{K}_{s\underset{\sim}{\lambda}}^T=\mathrm{diag}\left(\int_\Omega\boldsymbol{\Psi}^{\underset{\sim}{\lambda}T}\left(\widetilde{\boldsymbol{\partial}}_s\,\boldsymbol{\Psi}^u\right)\,\mathrm{d}\Omega,\,\boldsymbol{\Lambda}^T\right) \tag{61f}$$

$$\mathbf{K}_{\underset{\sim}{\lambda}\widetilde{\gamma}}=\mathbf{K}_{\widetilde{\gamma}\underset{\sim}{\lambda}}^T=\mathrm{diag}\left(\int_\Omega\boldsymbol{\Psi}^{\underset{\sim}{\lambda}T}\boldsymbol{\Psi}^{\widetilde{\gamma}}\,\mathrm{d}\Omega,\,\boldsymbol{\Upsilon}^T\right) \tag{61g}$$

$$\mathbf{f}=\int_\Omega\boldsymbol{\Psi}^{uT}\overline{\mathbf{b}}\,\mathrm{d}\Omega+\int_{\Gamma_t}\boldsymbol{\Psi}^{uT}\overline{\mathbf{t}}\,\mathrm{d}\Gamma_t\,,\quad \underset{\sim}{\widehat{\boldsymbol{\lambda}}}=\begin{Bmatrix}\underset{\sim}{\widehat{\boldsymbol{\lambda}}}^{\Omega}\\ \underset{\sim}{\widehat{\boldsymbol{\lambda}}}^{\Gamma}\end{Bmatrix}, \tag{61h}$$

the functional discretization, for arbitrary variations of $\delta\widehat{\mathbf{u}}$, $\delta\widehat{\widetilde{\boldsymbol{\gamma}}}$ and $\delta\underset{\sim}{\widehat{\boldsymbol{\lambda}}}$, leads to the following system

$$\begin{bmatrix}\mathbf{K}_{ff} & \mathbf{O} & \mathbf{K}_{s\underset{\sim}{\lambda}}\\ \mathbf{O} & \mathbf{K}_{\widetilde{\gamma}\widetilde{\gamma}} & -\mathbf{K}_{\widetilde{\gamma}\underset{\sim}{\lambda}}\\ \mathbf{K}_{\underset{\sim}{\lambda}s} & -\mathbf{K}_{\underset{\sim}{\lambda}\widetilde{\gamma}} & \mathbf{O}\end{bmatrix}\begin{Bmatrix}\widehat{\mathbf{u}}\\ \widehat{\widetilde{\boldsymbol{\gamma}}}\\ \underset{\sim}{\widehat{\boldsymbol{\lambda}}}\end{Bmatrix}=\begin{Bmatrix}\mathbf{f}\\ \mathbf{0}\\ \mathbf{0}\end{Bmatrix}. \tag{62}$$

Taking into account that $\widehat{\widetilde{\boldsymbol{\gamma}}}$ and $\underset{\sim}{\widehat{\boldsymbol{\lambda}}}$ are internal degrees of freedom, they may be statically condensed. Thus, after solving the above system we are left with

$$\left(\mathbf{K}_{ff}+\left(\mathbf{K}_{\underset{\sim}{\lambda}\widetilde{\gamma}}^{-1}\,\mathbf{K}_{\underset{\sim}{\lambda}s}\right)^T\,\mathbf{K}_{\widetilde{\gamma}\widetilde{\gamma}}\,\left(\mathbf{K}_{\underset{\sim}{\lambda}\widetilde{\gamma}}^{-1}\,\mathbf{K}_{\underset{\sim}{\lambda}s}\right)\right)\,\widehat{\mathbf{u}}=\mathbf{f}\,. \tag{63}$$

By defining

$$\overline{\mathbf{K}}_{ss}=\left(\mathbf{K}_{\underset{\sim}{\lambda}\widetilde{\gamma}}^{-1}\,\mathbf{K}_{\underset{\sim}{\lambda}s}\right)^T\,\mathbf{K}_{\widetilde{\gamma}\widetilde{\gamma}}\,\left(\mathbf{K}_{\underset{\sim}{\lambda}\widetilde{\gamma}}^{-1}\,\mathbf{K}_{\underset{\sim}{\lambda}s}\right), \tag{64}$$

the equation (63) can be written as

$$\left(\mathbf{K}_{ff}+\overline{\mathbf{K}}_{ss}\right)\,\widehat{\mathbf{u}}=\mathbf{f}\,. \tag{65}$$

[1] Note that in this section is used $\widehat{\mathbf{u}}$ as an alternative to $\mathbf{d}$ as used in subsection 3.1. Given that there are two more approximations ($\boldsymbol{\lambda}$ and $\widetilde{\boldsymbol{\gamma}}$) besides the displacement approximation $\mathbf{u}$, we opted for the notation $\widehat{\mathbf{u}}$ in order to have consistency between the three approximations.

Therefore, we can say that using the traditional formulation is very similar to using formulation where the vector distortion $\boldsymbol{\gamma}$ is directly approximated. The only difference between them is that instead of $\mathbf{K}_{ss}$, we have $\overline{\mathbf{K}}_{ss}$. Thus, the mixed formulation can be used to interpret the selective integration. For the case of reduced integration, would also require weakening $\boldsymbol{\chi} = \boldsymbol{\partial_f}\,\mathbf{u}$. Evaluating $\mathbf{K}^{-1}_{\underset{\sim}{\lambda}\underset{\sim}{\tilde{\gamma}}}$ and $\mathbf{K}_{\underset{\sim}{\lambda}s}$, then $\overline{\mathbf{K}}_{ss}$ results in

$$\overline{\mathbf{K}}_{ss} = \left(\mathbf{K}^{-1}_{\underset{\sim}{\lambda}\underset{\sim}{\tilde{\gamma}}}\,\mathbf{K}_{\underset{\sim}{\lambda}s}\right)^T \mathbf{K}_{\tilde{\gamma}\tilde{\gamma}} \left(\mathbf{K}^{-1}_{\underset{\sim}{\lambda}\underset{\sim}{\tilde{\gamma}}}\,\mathbf{K}_{\underset{\sim}{\lambda}s}\right) = \left(\mathbf{K}^{-1}_{\underset{\sim}{\lambda}\underset{\sim}{\tilde{\gamma}}}\,\mathbf{K}_{\underset{\sim}{\lambda}s}\right)^T$$
$$\int_\Omega \left(\left[\mathbf{g}^1\,\mathbf{g}^2\right]\,\boldsymbol{\Psi}^{\tilde{\gamma}}\right)^T \mathbf{D}_s \left(\left[\mathbf{g}^1\,\mathbf{g}^2\right]\,\boldsymbol{\Psi}^{\tilde{\gamma}}\right)\mathrm{d}\Omega \left(\mathbf{K}^{-1}_{\underset{\sim}{\lambda}\underset{\sim}{\tilde{\gamma}}}\,\mathbf{K}_{\underset{\sim}{\lambda}s}\right) =$$
$$= \int_\Omega \left(\left[\mathbf{g}^1\,\mathbf{g}^2\right]\boldsymbol{\Psi}^{\tilde{\gamma}}\,\mathbf{K}^{-1}_{\underset{\sim}{\lambda}\underset{\sim}{\tilde{\gamma}}}\,\mathbf{K}_{\underset{\sim}{\lambda}s}\right)^T \mathbf{D}_s$$
$$\left(\left[\mathbf{g}^1\,\mathbf{g}^2\right]\boldsymbol{\Psi}^{\tilde{\gamma}}\,\mathbf{K}^{-1}_{\underset{\sim}{\lambda}\underset{\sim}{\tilde{\gamma}}}\,\mathbf{K}_{\underset{\sim}{\lambda}s}\right)\mathrm{d}\Omega = \int_\Omega \overline{\mathbf{B}}_s^T\,\mathbf{D}_s\,\overline{\mathbf{B}}_s\,\mathrm{d}\Omega\,. \quad (66)$$

where

$$\overline{\mathbf{B}}_s = \left[\mathbf{g}^1\,\mathbf{g}^2\right]\,\boldsymbol{\Psi}^{\tilde{\gamma}}\,\mathbf{K}^{-1}_{\underset{\sim}{\lambda}\underset{\sim}{\tilde{\gamma}}}\,\mathbf{K}_{\underset{\sim}{\lambda}s}\,, \quad (67)$$

4.3 Relation of mixed formulation with selective integration

Consider the Lagrangian isoparametric element with $(n\times n)$ nodes or the Serendipity element with $4(n-1)$ nodes, such that the Jacobian $|\mathbf{J}(\boldsymbol{\xi})|$ is constant, *i.e.*, the element is rectangular or parallelogram. Assume also that the constitutive operator $\mathbf{D}_s$ is also constant.

For the evaluation of the shear stiffness matrix we have

$$\mathbf{K}_{ss} = \int_\Omega \mathbf{B}_s^T\,\mathbf{D}_s\,\mathbf{B}_s\,\mathrm{d}\Omega = \int_{\widehat{\Omega}} \mathbf{B}_s^T\,\mathbf{D}_s\,\mathbf{B}_s\,|\mathbf{J}|\,\mathrm{d}\widehat{\Omega}\,,\widehat{\Omega} = [-1,1]^2\,. \quad (68)$$

Given that $\mathbf{B}_s$ is of $(n-1)$ degree in each direction, then the term $\mathbf{B}_s^T\,\mathbf{D_s}\,\mathbf{B}_s\,|\mathbf{J}|$ has is of $2(n-1)$ degree. Hence, for the exact integration of $\mathbf{B}_s^T\,\mathbf{D}_s\,\mathbf{B}_s$ would be needed, according to Gauss-Legendry rules, at least $(n-1)\times(n-1)$ Gauss points, *i.e.*,

$$\mathbf{K}_{ss}^{red} = \sum_{i=1}^{(n-1)^2} \left[\mathbf{B}_s^T\,\mathbf{D}_s\,\mathbf{B}_s\right]\big|_{\boldsymbol{\xi}=\boldsymbol{\xi}_i}\,|\mathbf{J}|\,w_i\,. \quad (69)$$

In the mixed form, we have

$$\overline{\mathbf{K}}_{ss} = \int_\Omega \overline{\mathbf{B}}_s^T\,\mathbf{D}_s\,\overline{\mathbf{B}}_s\,\mathrm{d}\Omega\,, \quad (??)$$

Assuming that $\mathbf{g}^1 \equiv \mathbf{e}_1$ and $\mathbf{g}^2 \equiv \mathbf{e}_2$, than $\left[\mathbf{g}^1\,\mathbf{g}^2\right] \equiv \mathbf{I}$, where $\mathbf{I}$ is the *Identity Matrix*, and the expression (67) takes the form

$$\overline{\mathbf{B}}_s = \boldsymbol{\Psi}^{\gamma}\,\mathbf{K}^{-1}_{\lambda\gamma}\,\mathbf{K}_{\lambda s}\,. \quad (70)$$

Considering again an isoparametric element QL with $(n\times n)$ nodes or element QS $4(n-1)$ nodes, under the same conditions set previously.

For this elements, it is assumed

$$\boldsymbol{\Psi}^{\lambda} = \begin{bmatrix}\boldsymbol{\Phi}^{\lambda} & \mathbf{O}\\ \mathbf{O} & \boldsymbol{\Phi}^{\lambda}\end{bmatrix} \quad \boldsymbol{\Psi}^{\gamma} = \begin{bmatrix}\boldsymbol{\Phi}^{\gamma} & \mathbf{O}\\ \mathbf{O} & \boldsymbol{\Phi}^{\gamma}\end{bmatrix}\,, \quad (71)$$

where

$$\boldsymbol{\Phi}^{\lambda} = \left[\Phi_1^{\lambda} \quad \Phi_2^{\lambda} \quad \ldots \quad \Phi^{\lambda}_{(n-1)^2}\right] =$$
$$= \left[\delta(\boldsymbol{\xi}-\boldsymbol{\xi}_1) \quad \delta(\boldsymbol{\xi}-\boldsymbol{\xi}_2) \quad \ldots \quad \delta\left(\boldsymbol{\xi}-\boldsymbol{\xi}_{(n-1)^2}\right)\right]\,, \quad (72)$$

$$\boldsymbol{\Phi}^{\gamma} = \left[\Phi_1^{\gamma} \quad \Phi_2^{\gamma} \quad \ldots \quad \Phi^{\gamma}_{(n-1)^2}\right]\,. \quad (73)$$

$\Phi_j^{\gamma}(\boldsymbol{\xi})$ are the interpolation functions with a degree $(n-2)$ in each direction, which satisfy the condition $\Phi_j^{\gamma}(\boldsymbol{\xi}_i) = \delta_{ij}$. These are obtained by the tensorial product of one-dimensional polynomials. $\boldsymbol{\xi}_i$ are the $(n-1)\times(n-1)$ Gauss rule points coordinates.

Setting $\mathbf{K}_{\lambda\gamma}$ as

$$\mathbf{K}_{\lambda\gamma} = \begin{bmatrix}\mathbf{K}^1_{\lambda\gamma} & \mathbf{O}\\ \mathbf{O} & \mathbf{K}^2_{\lambda\gamma}\end{bmatrix} \quad (74)$$

and taking in account the approximations of $\boldsymbol{\gamma}$ and $\boldsymbol{\lambda}$, it is obtained

$$\left(\mathbf{K}^1_{\lambda\gamma}\right)_{ij} = \left(\mathbf{K}^2_{\lambda\gamma}\right)_{ij} = \int_\Omega \delta(\boldsymbol{\xi}-\boldsymbol{\xi}_i)\,\Phi_j^{\gamma}(\boldsymbol{\xi})\,\mathrm{d}\Omega = \Phi_j^{\gamma}(\boldsymbol{\xi}_i) = \delta_{ij}, \quad (75)$$

which leads to

$$\mathbf{K}_{\lambda\gamma} = \int_\Omega \boldsymbol{\Psi}^{\lambda T}\,\boldsymbol{\Psi}^{\gamma}\,\mathrm{d}\Omega \equiv \mathbf{I}\,. \quad (76)$$

The matrix $\mathbf{K}_{\lambda s}$ can also be written as

$$\mathbf{K}_{\lambda s} = \int_\Omega \boldsymbol{\Psi}^{\lambda T}\,\mathbf{B}_s\,\mathrm{d}\Omega = \begin{bmatrix}\mathbf{B}_s|_{\boldsymbol{\xi}=\boldsymbol{\xi}_1}\\ \mathbf{B}_s|_{\boldsymbol{\xi}=\boldsymbol{\xi}_2}\\ \vdots\\ \mathbf{B}_s|_{\boldsymbol{\xi}=\boldsymbol{\xi}_{(n-1)^2}}\end{bmatrix} \quad (77)$$

Thus, the expression (70) becomes

$$\overline{\mathbf{B}}_s = \boldsymbol{\Psi}^{\gamma}\,\mathbf{K}^{-1}_{\lambda\gamma}\,\mathbf{K}_{\lambda s} = \boldsymbol{\Psi}^{\gamma}\,\mathbf{I}^{-1}\begin{bmatrix}\mathbf{B}_s|_{\boldsymbol{\xi}=\boldsymbol{\xi}_1}\\ \mathbf{B}_s|_{\boldsymbol{\xi}=\boldsymbol{\xi}_2}\\ \vdots\\ \mathbf{B}_s|_{\boldsymbol{\xi}=\boldsymbol{\xi}_{(n-1)^2}}\end{bmatrix} =$$
$$= \Phi_1^{\gamma}\;\mathbf{B}_s|_{\boldsymbol{\xi}=\boldsymbol{\xi}_1} + \ldots + \Phi^{\gamma}_{(n-1)^2}\;\mathbf{B}_s|_{\boldsymbol{\xi}=\boldsymbol{\xi}_{(n-1)^2}} =$$
$$= \sum_{i=1}^{(n-1)^2} \Phi_i^{\gamma}\;\mathbf{B}_s|_{\boldsymbol{\xi}=\boldsymbol{\xi}_i}\,. \quad (78)$$

Then

$$\overline{\mathbf{K}}_{ss} = \int_\Omega \overline{\mathbf{B}}_s^T\,\mathbf{D}_s\,\overline{\mathbf{B}}_s\,\mathrm{d}\Omega = \int_{\widehat{\Omega}} \overline{\mathbf{B}}_s^T\,\mathbf{D}_s\,\overline{\mathbf{B}}_s\,|\mathbf{J}|\,\mathrm{d}\widehat{\Omega} =$$
$$= \begin{bmatrix}\mathbf{B}_s|_{\boldsymbol{\xi}=\boldsymbol{\xi}_1}\\ \mathbf{B}_s|_{\boldsymbol{\xi}=\boldsymbol{\xi}_2}\\ \vdots\\ \mathbf{B}_s|_{\boldsymbol{\xi}=\boldsymbol{\xi}_{(n-1)^2}}\end{bmatrix}^T \int_{\widehat{\Omega}} \boldsymbol{\Phi}^{\gamma T}\,\mathbf{D}_s\,\boldsymbol{\Phi}^{\gamma}\,|\mathbf{J}|\,\mathrm{d}\widehat{\Omega} \begin{bmatrix}\mathbf{B}_s|_{\boldsymbol{\xi}=\boldsymbol{\xi}_1}\\ \mathbf{B}_s|_{\boldsymbol{\xi}=\boldsymbol{\xi}_2}\\ \vdots\\ \mathbf{B}_s|_{\boldsymbol{\xi}=\boldsymbol{\xi}_{(n-1)^2}}\end{bmatrix}. \quad (79)$$

Knowing that $\mathbf{\Phi}^{\gamma}$ has a degree $(n-2)$ in each direction, then the term $\mathbf{\Phi}^{\gamma T}\,\mathbf{D}_s\,\mathbf{\Phi}^{\gamma}\,|\mathbf{J}|$ has a degree $2(n-2)$, and will be needed $(n-1)$ points to exactly integrate it in each direction

$$\int_{\widehat{\Omega}} \mathbf{\Phi}^{\gamma T}\,\mathbf{D}_s\,\mathbf{\Phi}^{\gamma}\,|\mathbf{J}|\,\mathrm{d}\widehat{\Omega} = \sum_{i=1}^{(n-1)^2} \left[\mathbf{\Psi}^{\gamma T}\,\mathbf{D}_s\,\mathbf{\Psi}^{\gamma}\right]\Big|_{\boldsymbol{\xi}=\boldsymbol{\xi}_i} |\mathbf{J}|\,w_i\,. \tag{80}$$

Setting $\mathbf{\Psi}^{\gamma T}\,\mathbf{D}_s\,\mathbf{\Psi}^{\gamma}$ as

$$\mathbf{\Psi}^{\gamma T}\,\mathbf{D}_s\,\mathbf{\Psi}^{\gamma} = \begin{bmatrix} \mathbf{\Phi}^{\gamma T}\,\mathbf{D}_s\,\mathbf{\Phi}^{\gamma} & \mathbf{O} \\ \mathbf{O} & \mathbf{\Phi}^{\gamma T}\,\mathbf{D}_s\,\mathbf{\Phi}^{\gamma} \end{bmatrix}, \tag{81}$$

where

$$\mathbf{\Phi}^{\gamma T}\,\mathbf{D}_s\,\mathbf{\Phi}^{\gamma} = \begin{bmatrix} \Phi^{\gamma}_1\,D_s\,\Phi^{\gamma}_1 & \Phi^{\gamma}_1\,D_s\,\Phi^{\gamma}_2 & \dots & \Phi^{\gamma}_1\,D_s\,\Phi^{\gamma}_{(n-1)} \\ \Phi^{\gamma}_2\,D_s\,\Phi^{\gamma}_1 & \Phi^{\gamma}_2\,D_s\,\Phi^{\gamma}_2 & \dots & \Phi^{\gamma}_2\,D_s\,\Phi^{\gamma}_{(n-1)} \\ \vdots & \vdots & \ddots & \vdots \\ \Phi^{\gamma}_{(n-1)}\,D_s\,\Phi^{\gamma}_1 & \Phi^{\gamma}_{(n-1)}\,D_s\,\Phi^{\gamma}_2 & \dots & \Phi^{\gamma}_{(n-1)}\,D_s\,\Phi^{\gamma}_{(n-1)} \end{bmatrix} \tag{82}$$

and noticing that $[\Phi^{\gamma}_m\,D_s\,\Phi^{\gamma}_n]|_{\boldsymbol{\xi}=\boldsymbol{\xi}_i} = \Phi^{\gamma}_m\,(\boldsymbol{\xi}_i)\;D_s\,\Phi^{\gamma}_n\,(\boldsymbol{\xi}_i) = \delta_{mi}\,D_s\,\delta_{ni} = \delta_{mn}\,D_s$, than the evaluation of $\overline{\mathbf{K}}_{ss}$ comes down to

$$\overline{\mathbf{K}}_{ss} = \begin{bmatrix} \mathbf{B}_s|_{\boldsymbol{\xi}=\boldsymbol{\xi}_1} \\ \mathbf{B}_s|_{\boldsymbol{\xi}=\boldsymbol{\xi}_2} \\ \vdots \\ \mathbf{B}_s|_{\boldsymbol{\xi}=\boldsymbol{\xi}_{(n-1)^2}} \end{bmatrix}^T \begin{bmatrix} w_1 & 0 & \dots & \\ 0 & w_2 & 0 & \dots \\ \vdots & 0 & \ddots & \end{bmatrix} D_s\,|\mathbf{J}| \begin{bmatrix} \mathbf{B}_s|_{\boldsymbol{\xi}=\boldsymbol{\xi}_1} \\ \mathbf{B}_s|_{\boldsymbol{\xi}=\boldsymbol{\xi}_2} \\ \vdots \\ \mathbf{B}_s|_{\boldsymbol{\xi}=\boldsymbol{\xi}_{(n-1)^2}} \end{bmatrix} = \sum_{i=1}^{(n-1)^2} \left[\mathbf{B}_s^T\,\mathbf{D}_s\mathbf{B}_s\right]\Big|_{\boldsymbol{\xi}=\boldsymbol{\xi}_i} |\mathbf{J}|\,w_i\,. \tag{83}$$

Noticing equality between expressions (69) and (83) it is concluded that $\mathbf{K}^{red}_{ss} = \overline{\mathbf{K}}_{ss}$. That is, the selective integration of quadrilateral isoparametric elements is the same as mixed formulation, assuming certain approximations for $\boldsymbol{\gamma}$ and $\boldsymbol{\lambda}$. Therefore, selective integration can be viewed as elements with substitute shear strain fields (Hinton and Huang, 1986).

4.4 MITC elements

The formulation previously made in subsection 4.2 is general and can be applied to any element. Several MITC elements were proposed in the last decades (Dvorkin and Bathe, 1984; Bathe, 1996). The main distinction between each one of them are described in terms of elementary approximations $\mathbf{\Psi}^{u}$, $\mathbf{\Psi}^{\widetilde{\gamma}}$ and $\mathbf{\Psi}^{\lambda}$.

The approximation functions $\mathbf{\Psi}^{\widetilde{\gamma}}$ are generated differently, and have different formats depending on the type of element.

Depending on the definition of $\mathbf{\Psi}^{\lambda}$, different kinds of restrictions are imposed:

1. when used $\Phi^{\lambda\alpha}_i = \delta(\boldsymbol{\xi}-\boldsymbol{\xi}^{\alpha}_i)$, where $\delta(\boldsymbol{\xi}-\boldsymbol{\xi}^{\alpha}_i)$ is the Dirac function concentrated at $\boldsymbol{\xi}^{\alpha}_i$, the integral restrictions imposed on the functional (56) degenerate in discrete constrains because

$$\int_{-\infty}^{+\infty} f\,(\boldsymbol{\xi})\;\delta\,(\boldsymbol{\xi}-\boldsymbol{\xi}_i)\;\mathrm{d}\xi = f\,(\boldsymbol{\xi}_i)\;. \tag{84}$$

   Thus we obtain a *discrete restriction*. Points $\boldsymbol{\xi}^{\alpha}_i$ are sometimes called *tying points*.

2. in case of using $\Phi^{\lambda\alpha} = p_{\alpha}\,(\boldsymbol{\xi})$, where $p_{\alpha}\,(\boldsymbol{\xi})$ is a polinomial function in the α direction, we get a *integral restriction*.

It should also be noted that the third term of the second member of the equation (56), $\sum_{i=1}^{n} \widehat{\lambda}^{\Gamma}_i\,\left[(\boldsymbol{\gamma}-\boldsymbol{\gamma}^{DI})\cdot\mathbf{t}\right]\big|_{\boldsymbol{\xi}=\boldsymbol{\xi}_i}$, will only be considered in MITCp triangular case.

Next, we will show the several MITC elements studied in this work and its characteristics, including degrees of freedom at each node, *tying points* location and the approximation functions. In the case of quadrilateral elements, the *tying points* and approximation functions $\mathbf{\Phi}^{\lambda\alpha}$ and $\mathbf{\Phi}^{\widetilde{\gamma}_{\alpha}}$ will only appear in the direction ξ_1 , since everything is identical in the perpendicular direction by simply replacing ξ_1 by ξ_2.

5 Numerical examples

In terms of the elements application, it was chosen a problem for which it is possible to know the exact solutions of the several types for analysis, allowing the assessment of the quality of the approaches made by each element. Hence, a rectangular simply supported plate (support type *Hard*) with dimensions (4×2) is tested. In order to reduce the computational cost and processing time data, two symmetry simplification are made, resulting in a rectangular plate of dimension (2×1), with two sliding clamped edges in the symmetry axes. The adopted physical properties were $h = 0,20$, $E = 2\times 10^8$, $\nu = 0,3$ and $\rho = 1$, in a consistent system of units. The adimensionalized thickness is defined by the ratio h/L, being $L = 2$.

5.1 Static analysis

Patch test

The standard bending, shear and twisting *patch tests* (Hinton and Huang, 1986) were conducted for all MITC elements. All of them exactly pass the three tests, except the MITC9p for the bending and twisting tests. In this latter case these tests are almost fulfilled.

Convergence test

As mentioned above, in order to evaluate the efficiency of each component and the quality of the FEM solution for moderately thick rectangular plate with a unit uniform

Element type	number of nodes	Mesh	
		regular	distorted
MITCp	4	0,99	0,93
	9	2,10	2,02
	16	2,97	2,44
	7	1,97	1,77
	12	2,96	2,95
MITCs	9	2,00	2,02
	16	2,79	2,59

Table 1: Convergence rate for the strain energy of the MITC elements, using regular and distorted meshes, for the studied case.

load, $\overline{p} = 1$, it is necessary to compare the numerical values obtained for the given mesh of the elements under study with the exact values.

Firstly, regular and distorted meshes for the various types of conventional finite elements were tested, by varying the characteristic dimension of the elements, h, and evaluating the norm of the error associated to the strain energy, $\|\mathbf{e}_h\|_E = \|\mathbf{u} - \mathbf{u}_h\|_E$. The average slopes of the several generated graphics of strain energy error as a function of the characteristic dimension of the elements are presented on Tables 1 and 2. By directly comparing the results obtained in the regular meshes and distorted, it is possible to conclude that all elements — MITC and conventional — showed better convergence rates and more accurate results when not distorted. We also can conclude that increasing the order of the element, in each family type, the solution is improved, getting, element by element, convergence rates one unit higher, since the maximum degree of the polynomial complete function is also one unit higher. However in Serendipity elements, it was shown that there is no advantage to choose an element of a higher order than QS12, since the complete approximation function never exceeds the 3rd degree. It can also be seen from Tables 1 and 2, that MITC elements, generally have higher rates: QL4 and MITC4 are characterized by very similar results, the MITC9p has higher rates than the QL9 as the triangular elements, MITC7p and MITC12p, comparing to the elements T6 and T10, respectively. However, the convergence rate of the strain energy is not the only criterion for performance comparison of finite elements. To obtain the results discussed below it was considered a thickness of $h/L = 0.025$. As it can be seen in Figures 1 and 2 that MITC4 presents better results in the representation of the of shear component v_1 than QL4, especially when a distorted mesh is employed.

On the other hand, in the representation of m_{11}, the two elements show the same performance. The Figure 3 support the previous statement. About the convergence of the adimensional displacement, w/w_e, in the middle of the plate, the results are presented in Figures 4. Thus, for $h/L = 0.025$, the results obtained using the complete inte-

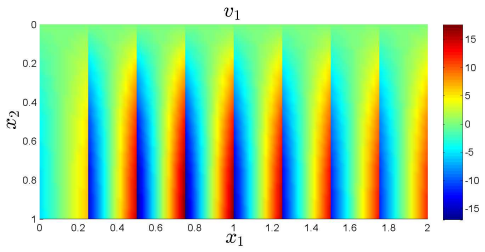

(a) QL4

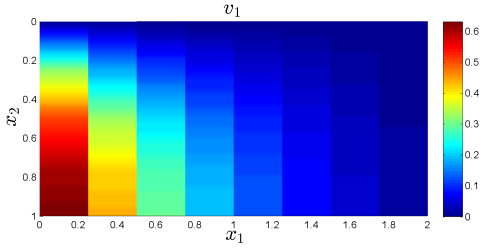

(b) MITC4

Figure 1: Results obtained for the shear component v_1, using selective integration, in the case of a 32 elements regular mesh.

gration in QL4 were worse than MITC4. However, when using the selective integration, the results of the displacement for the two elements are visually coincident. Using the reduced integration, the results of element QL4 are slightly closer to the exact solution. Identical conclusions would be obtained if this assessment was made in terms of strain energy, because the resulting graphics would be similar.

It was also calculated the time spent, per element, by the program to form the stiffness matrix, the equivalent nodal load vector, to make the axis rotation to the local referential and the assembly process. Through the observation of the Figure 5, it can be stated that the MITC elements, quadrilateral and triangular, have a higher computational cost comparing to conventional elements of the same order.

Shear-Locking

The second test for the statical analysis pretended to assess the elements behavior when the thickness of the plate tended to zero, *i.e.*, their sensitivity to *shear-locking*. Thus, we evaluated the evolution of the normalized value of the maximum transverse displacement at the middle of the plate, w/w_e, *versus* the ratio L/h. In this analysis we used the regular mesh of 32 elements. Despite the fact that they are Reissner-Mindlin elements, it's expected that as the plate thickness decreases, the results converge to solutions provided by Kirchhoff's theory. From the observation of Figures 6, 7, 8 we can say, for this particular example, that the *shear-locking* phenomenon was only activated in conventional elements T3, T6 and QL4 using full integration and quadrilateral Serendipity for the considered mesh (32 elements). However, it is suspected that the activation

Element type	number of nodes	Mesh					
		Regular			Distorted		
		Integration			Integration		
		complete	selective	reduced	complete	selective	reduced
QL	4	0,91	1,00	1,00	0,71	0,94	0,95
	9	1,96	2,00	2,01	1,75	1,92	1,94
	16	2,94	2,91	3,09	2,58	2,71	2,69
	25	3,37	3,25	4,03	2,62	3,18	2,40
	36	3,13	2,84	3,45	1,83	1,92	1,81
QS	8	1,96	2,03	2,05	1,79	2,20	2,25
	12	2,89	2,91	2,92	2,68	2,73	2,73
	16	2,92	2,92	2,92	2,68	2,72	2,72
	20	2,92	2,92	2,92	2,68	2,72	2,72
T	3	0,90	—	—	0,53	—	—
	6	1,97	—	—	1,71	—	—
	10	2,87	—	—	2,50	—	—
	15	3,77	—	—	2,65	—	—
	21	2,97	—	—	2,57	—	—

Table 2: Convergence rate for the strain energy of the different conventional elements with different types of integrations, using regular and distorted meshes, to the studied case.

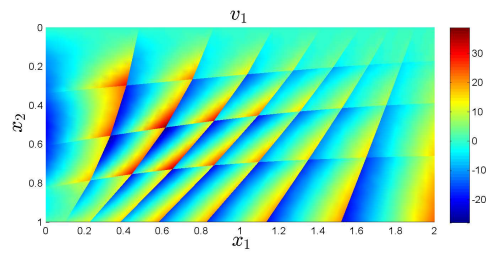

(a) QL4

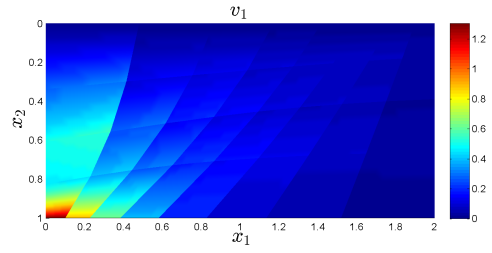

(b) MITC4

Figure 2: Results obtained for the shear component v_1, in the case of a 32 elements distorted mesh.

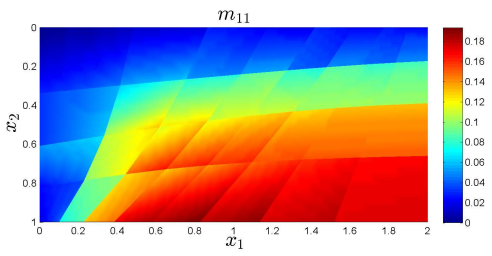

(a) QL4

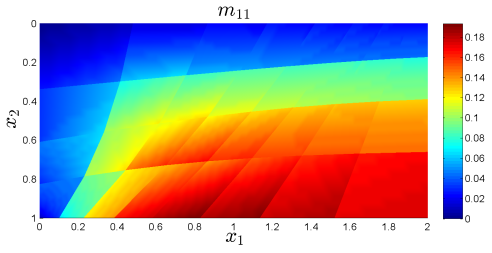

(b) MITC4

Figure 3: Results obtained for m_{11}, using selective integration, in the case of a 32 elements distorted mesh.

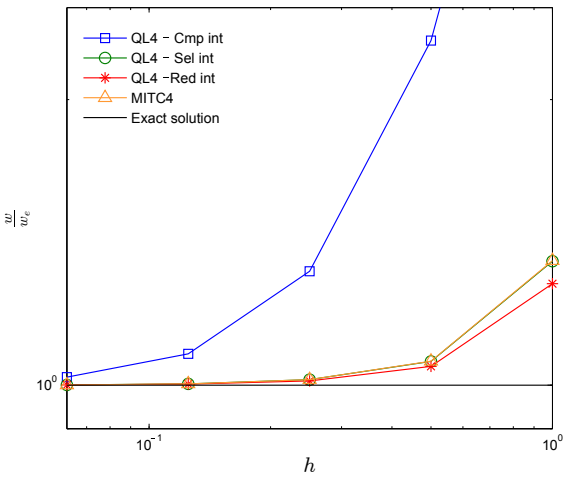

Figure 4: Results obtained for the adimensional displacement, w/w_e, in the middle of the plate, using MITC4 and using QL4 with several types of integration.

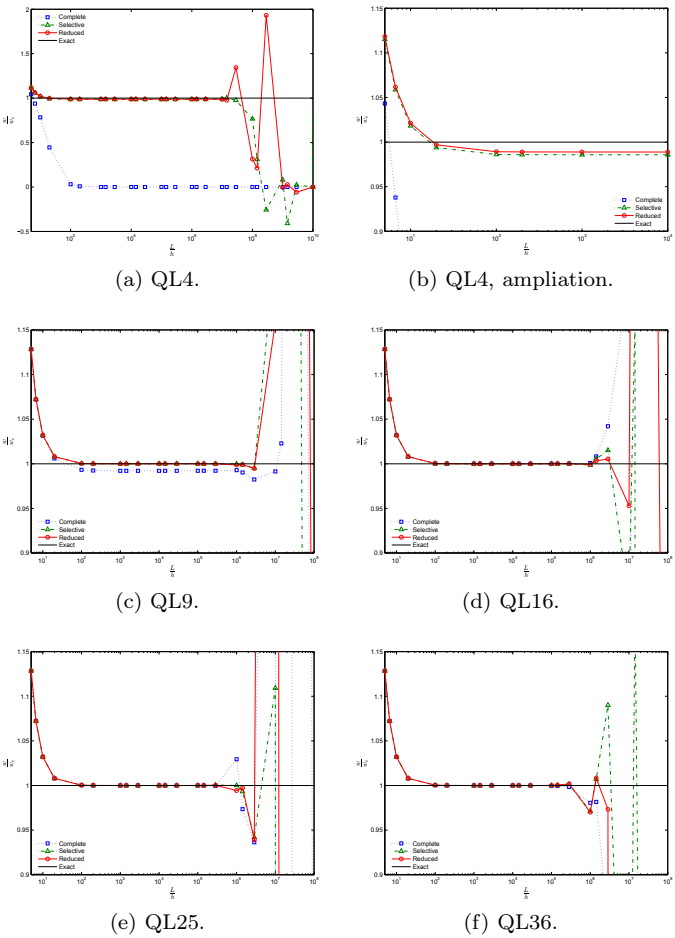

(a) QL4. (b) QL4, ampliation.

(c) QL9. (d) QL16.

(e) QL25. (f) QL36.

Figure 6: *Shear-locking* of the Lagrangian elements.

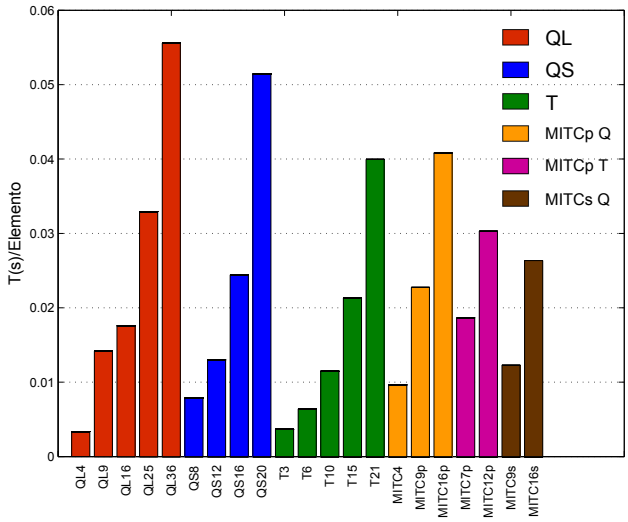

Figure 5: Computational time spent by the program, per element, in the formation of elementar matrices and its assembly.

of this phenomenon was not found in other conventional elements as this only would occur after the appearance of the erratic behavior caused by the limited accuracy of the machine. For a mesh of 512 elements, using full integration in elements T6 and Serendipity the *shear-locking* phenomenon is activated for higher ratios of L/h than the ones using a mesh of 32 elements. This phenomenon can be explained by the fact that the elements, after refinement of the mesh have a greater thickness/characteristic dimension ration, so that they tend to behave as moderately thick elements, making the theory of Reissner-Mindlin valid. In the MITC elements (Figure 9) there is no trace of *shear-locking*, even for the lowest order element, MITC4, and unlike conventional elements, this phenomenon should not occur after the numerical errors. For these elements and for the conventional elements that had shown no trace of activation of *shear-locking* it was found that when the ratio L/h increases, the results converge to a given solution close to exact one, depending on to the order of the element, number of elements used in the mesh and the type of integration used. Hence, it can be said that for these elements, the convergence of the solution provided to the Kirchhoff's theory is as good as desired, depending on the mesh refinement

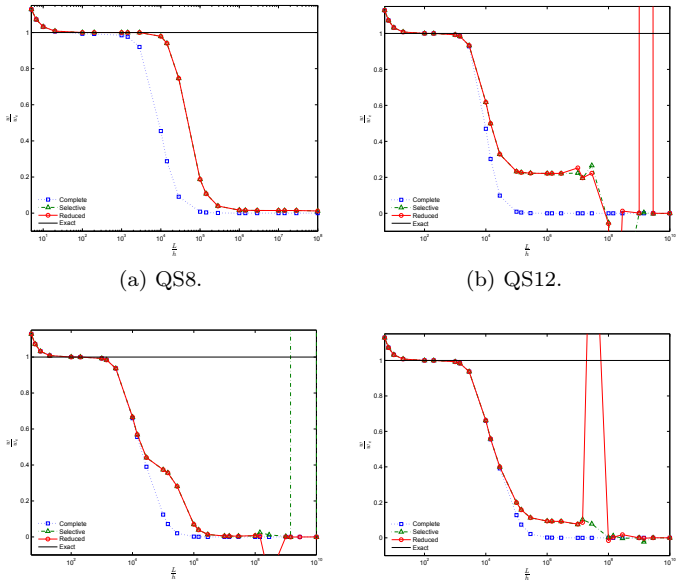

(a) QS8. (b) QS12.

(c) QS16. (d) QS20.

Figure 7: *Shear-locking* of the Serendipity elements.

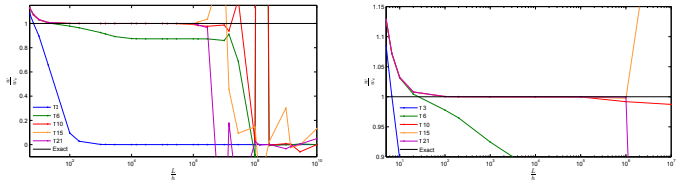

(a) T. (b) T, ampliation.

Figure 8: *Shear-locking* of the triangular elements.

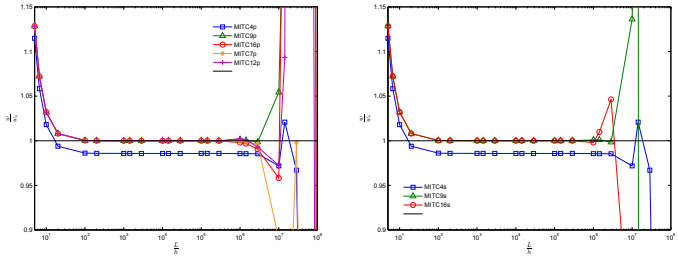

(a) MITCp. (b) MITCs.

Figure 9: *Shear-locking* of MITC elements.

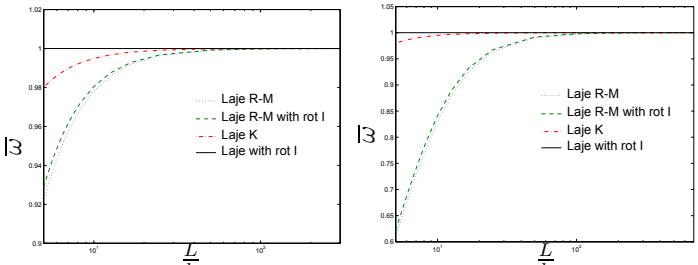

(a) Fundamental mode. (b) Sixth mode.

Figure 10: Adimensional frequency vibrations. In the case of the Reissner-Mindlin elements, a regular mesh with 128 MITC16p elements was used.

used for each element type and each integration rule.

Free-vibration analysis

For the free vibration analysis, it was evaluated the convergence of the numerical values of the natural vibration frequency obtained from the study of the finite elements with respect to the exact solution. The results obtained using the finite elements are presented on Tables 3 and 4. Selective integration was employed in the case of conventional elements.

For each mode, one may conclude that increasing the order of the element, in each family type, the solution is improved, getting, element by element, convergence rates one unit higher, since the maximum degree of the polynomial complete function is also one unit higher. However, once again, it is shown that it isn't worthwhile to use a Serendipity element higher than QS12. Furthermore, for the higher modes, the convergence rates tends, in general, to slightly decrease, which can be explained by the greater difficulty of representing these modes. In contrast to what is usual in the literature, in the present formulation, in addition to the usual terms of the inertia associated to the translation, it was also considered the related terms associated with the rotation. Thus, it was possible to carry out a study to assess its importance in the behavior of the vibration of the plate. For each of the plate theories (moderately thick and thin) it was found that this influence is smaller, as the plate becomes thinner. Besides, the frequency vibration values obtained are smaller for the same ratio h/L, when considering the terms in question, since in these situations the number of terms due to the mass is higher. This statements are supported by the results presented in Figure 10.

Linear stability analysis

The problem of linear stability analysis shows a similar format to the problem of free vibration analysis: consists in solving a problem of eigenvalues and eigenvectors. However the geometric matrix has a fundamental difference for the mass matrix: in its definition appear first derivatives

Element type	number of nodes	Modes					
		1	2	3	4	5	6
QL	4	2,08	2,14	2,39	2,22	2,33	2,05
	9	3,97	3,93	3,90	3,90	3,89	3,67
	16	5,95	5,94	5,84	5,78	5,78	5,72
	25	7,97	7,90	7,74	7,72	7,77	7,66
	36	6,39	9,86	9,63	9,63	9,69	9,53
QS	8	4,03	4,30	3,97	3,90	3,99	3,89
	12	6,94	6,29	6,12	5,79	6,02	5,76
	16	6,16	6,17	6,32	6,44	6,42	6,43
	20	6,84	6,31	6,25	6,04	6,00	6,23
T	3	1,77	1,75	2,10	2,08	1,94	1,91
	6	3,80	3,78	3,62	3,71	3,59	3,61
	10	6,07	5,69	5,77	5,74	5,65	5,57
	15	7,97	7,87	7,41	7,46	7,41	7,31
	21	9,76	9,27	9,77	9,72	9,49	9,45

Table 3: Convergence rate for frequency vibration, using conventional elements, for the studied case.

Element type	number of nodes	Modes					
		1	2	3	4	5	6
MITCp	4	2,03	2,16	2,45	2,35	2,35	2,05
	9	3,94	3,90	3,83	3,68	3,79	3,81
	16	6,17	5,99	5,49	5,69	5,69	5,42
	7	3,94	3,87	3,59	3,68	3,74	3,62
	12	5,48	5,93	5,85	5,86	5,68	5,63
MITCs	9	3,97	3,94	3,91	3,90	3,90	3,73
	16	5,20	5,94	5,84	5,78	5,78	5,72

Table 4: Convergence rate for frequency vibration, using MITC elements, for the studied case.

Element type	number of nodes	Modes					
		1	2	3	4	5	6
QL	4	2,01	2,02	2,07	2,10	2,03	2,05
	9	3,99	3,99	3,96	3,95	3,95	3,94
	16	5,93	5,92	5,82	5,78	5,77	5,71
	25	7,90	7,89	7,69	7,96	7,78	7,79
	36	6,62	9,85	9,59	10,15	9,52	9,45
QS	8	3,99	4,03	4,00	3,93	4,03	3,97
	12	6,07	6,06	6,08	6,00	5,94	5,95
	16	5,91	6,07	6,13	5,58	5,19	5,16
	20	6,07	6,17	6,28	5,95	5,87	6,41
T	3	1,96	1,91	1,95	2,01	1,97	1,91
	6	3,97	3,96	3,94	3,95	3,93	3,92
	10	5,96	5,97	5,96	5,97	5,96	5,93
	15	7,82	7,84	7,80	7,81	7,78	7,79
	21	8,96	9,78	9,66	10,05	9,61	9,50

Table 5: Convergence rates for instability loads, using conventional elements, for the studied case.

of the approximation functions and not the approximation functions *per se*. Thus, generally, the results are similar and the elements tend to the same theoretical convergence rates, Tables 5 and 6. Selective integration was employed in the case of conventional elements.

The behavior of the elements in the various modes may also be extrapolated from the first mode of instability, despite the approximation quality begins to deteriorate for higher modes. However, when using selective or reduced integration in Lagrangian elements, in this analysis, it is necessary to make a careful selection of the obtained modes from the program, since the selective integration of these particular elements is associated to an activation of spurious modes. The frequencies associated to these modes are totally erroneous. This behavior does not occur in Serendipity elements. When full integration is used, this problem ceases to exist, but the accuracy of the results and convergence rates of approximation errors are lower than the ones obtained with selective integration. The differences between the results of the two types of integration will increase as the plate gets thinner. In the MITC elements we don't have this kind of problem.

6 Conclusions

The mixed finite element formulation can be understood as an extension of the principle of stationarity of the total potential energy, where we have as variables generalized streeses and deformations, besides the displacements. In this paper, we present a formulation based on mixed fields $\mathbf{u}$, $\widetilde{\boldsymbol{\gamma}}$ and $\underset{\sim}{\boldsymbol{\lambda}}$. This mixed formulation led to a general form to evaluate the stiffness matrix $\overline{\mathbf{K}}_{ss}$, valid for all three types of MITC elements. Thus, it was concluded that using the traditional formulation is very similar to use a mixed formulation where the distortion vector, $\boldsymbol{\gamma}$, is directly approximated. The only difference is that, instead of $\mathbf{K}_{ss}$, it's used $\overline{\mathbf{K}}_{ss}$.

The mixed formulation also explains the use of selective integration in conventional quadrilateral elements. It can be demonstrated for these elements that $\mathbf{K}_{ss}^{red} = \overline{\mathbf{K}}_{ss}$, which means that the selective integration is not more than the mixed formulation of these elements assuming certain approximation functions for $\boldsymbol{\gamma}$ and $\boldsymbol{\lambda}$. Although this result is well known for other types of alternative formulations, the deduction presented here is original.

However, despite the selective integration of conventional quadrilateral elements have the same variational bases that the MITC elements, their functions approximations to $\boldsymbol{\gamma}$ and $\boldsymbol{\lambda}$ are different. It should be noted that sometimes, the first ones present spurious modes, while the seconds don't. Hence, it can be said that the mixed formulation is dependent on the choice of the approximation functions.

Summing up the numerical results, it can be stated that the MITC elements, despite the higher computational cost, have several advantages over conventional elements:

(i) they don't suffer from *shear-locking*;

(ii) they don't display spurious modes;

(iii) all elements, except element MITC9p, pass the bending, shear and twisting patch tests. In the case the MITC9p, the test is almost passed;

(iv) the representation of the shear components on static analysis converges quickly to the exact solution;

(v) show a slightly higher rate of convergence in terms of the norm of the strain energy error.

These conclusions remain valid regardless of the degree of distortion of the mesh considered.

A MITC approximation functions

Approximation functions for MITC9p:

$$\boldsymbol{\Psi}^{u} = \begin{bmatrix} \boldsymbol{\Psi}^{QS8} & \mathbf{O} & \mathbf{O} \\ \mathbf{O} & \boldsymbol{\Psi}^{QL9} & \mathbf{O} \\ \mathbf{O} & \mathbf{O} & \boldsymbol{\Psi}^{QL9} \end{bmatrix} \tag{85a}$$

$$\boldsymbol{\Phi}^{\widetilde{\gamma}_1} = \begin{bmatrix} 1 & \xi_1 & \xi_2 & \xi_1\xi_2 & \xi_2^2 \end{bmatrix} \tag{85b}$$

$$\boldsymbol{\Phi}^{\underset{\sim}{\lambda}_1} = \begin{bmatrix} \delta(\boldsymbol{\xi}-\boldsymbol{\xi}_1) & \delta(\boldsymbol{\xi}-\boldsymbol{\xi}_2) & \delta(\boldsymbol{\xi}-\boldsymbol{\xi}_3) & \delta(\boldsymbol{\xi}-\boldsymbol{\xi}_4) & 1 \end{bmatrix}. \tag{85c}$$

Approximation functions for MITC16p:

$$\boldsymbol{\Psi}^{u} = \begin{bmatrix} \boldsymbol{\Psi}^{w,M16p} & \mathbf{O} & \mathbf{O} \\ \mathbf{O} & \boldsymbol{\Psi}^{QL16} & \mathbf{O} \\ \mathbf{O} & \mathbf{O} & \boldsymbol{\Psi}^{QL16} \end{bmatrix} \tag{86a}$$

$$\boldsymbol{\Phi}^{\widetilde{\gamma}_1} = \begin{bmatrix} 1 & \xi_1 & \xi_2 & \xi_1^2 & \xi_1\xi_2 & \xi_2^2 & \xi_1^2\xi_2 & \xi_1\xi_2^2 & \xi_2^3 \end{bmatrix} \tag{86b}$$

$$\boldsymbol{\Phi}^{\underset{\sim}{\lambda}_1} = \begin{bmatrix} \delta(\boldsymbol{\xi}-\boldsymbol{\xi}_1) & \delta(\boldsymbol{\xi}-\boldsymbol{\xi}_2) & \delta(\boldsymbol{\xi}-\boldsymbol{\xi}_3) & \delta(\boldsymbol{\xi}-\boldsymbol{\xi}_4) & \delta(\boldsymbol{\xi}-\boldsymbol{\xi}_5) & \delta(\boldsymbol{\xi}-\boldsymbol{\xi}_6) & 1 & \xi_1 & \xi_2 \end{bmatrix}. \tag{86c}$$

Approximation functions for MITC7p:

$$\boldsymbol{\Psi}^{u} = \begin{bmatrix} \boldsymbol{\Psi}^{T6} & \mathbf{O} & \mathbf{O} \\ \mathbf{O} & \boldsymbol{\Psi}^{\theta,M7p} & \mathbf{O} \\ \mathbf{O} & \mathbf{O} & \boldsymbol{\Psi}^{\theta,M7p} \end{bmatrix} \tag{87a}$$

$$\boldsymbol{\Psi}^{\widetilde{\gamma}} = \begin{bmatrix} 1 & \xi_1 & \xi_2 & 0 & 0 & 0 & \xi_1\xi_2 & \xi_2^2 \\ 0 & 0 & 0 & 1 & \xi_1 & \xi_2 & -\xi_1^2 & -\xi_1\xi_2 \end{bmatrix} \tag{87b}$$

$$\boldsymbol{\Psi}^{\underset{\sim}{\lambda}} = \begin{bmatrix} \delta(\boldsymbol{\xi}-\boldsymbol{\xi}_1) & \delta(\boldsymbol{\xi}-\boldsymbol{\xi}_2) & -\frac{\sqrt{2}}{2}\delta(\boldsymbol{\xi}-\boldsymbol{\xi}_3) & \cdots \\ 0 & 0 & \frac{\sqrt{2}}{2}\delta(\boldsymbol{\xi}-\boldsymbol{\xi}_3) & \cdots \end{bmatrix}$$
$$\begin{matrix} -\frac{\sqrt{2}}{2}\delta(\boldsymbol{\xi}-\boldsymbol{\xi}_4) & 0 & 0 & 1 & 0 \\ \frac{\sqrt{2}}{2}\delta(\boldsymbol{\xi}-\boldsymbol{\xi}_4) & -\delta(\boldsymbol{\xi}-\boldsymbol{\xi}_5) & \delta(\boldsymbol{\xi}-\boldsymbol{\xi}_6) & 0 & 1 \end{matrix}\Bigg]. \tag{87c}$$

Element type	number of nodes	Modes					
		1	2	3	4	5	6
MITCp	4	2,12	2,27	2,07	2,10	2,10	2,13
	9	3,92	3,87	3,87	3,85	3,75	3,91
	16	5,95	5,86	5,80	5,81	5,94	5,10
	7	3,95	3,91	3,76	3,63	3,66	3,51
	12	6,18	6,13	5,83	6,04	5,35	5,29
MITCs	9	3,96	3,93	3,91	3,93	3,93	3,70
	16	5,89	5,92	5,82	5,78	5,76	5,71

Table 6: Convergence rates for instability loads, using MITC elements, for the studied case.

Approximation functions for MITC12p:

$$\boldsymbol{\Psi}^{u} = \begin{bmatrix} \boldsymbol{\Psi}^{T10} & \mathbf{O} & \mathbf{O} \\ \mathbf{O} & \boldsymbol{\Psi}^{\theta,M12p} & \mathbf{O} \\ \mathbf{O} & \mathbf{O} & \boldsymbol{\Psi}^{\theta,M12p} \end{bmatrix} \tag{88a}$$

$$\boldsymbol{\Psi}^{\tilde{\gamma}} = \begin{bmatrix} 1 & \xi_1 & \xi_2 & \xi_1^2 & \xi_1\xi_2 & \xi_2^2 & 0 & 0 & 0 & 0 \\ 0 & 0 & 0 & 0 & 0 & 0 & 1 & \xi_1 & \xi_2 & \xi_1^2 \cdots \end{bmatrix} \\ \begin{matrix} 0 & 0 & \xi_1^2\xi_2 & \xi_1\xi_2^2 & \xi_2^3 \\ \cdots \xi_1\xi_2 & \xi_2^2 & -\xi_1^3 & -\xi_1^2\xi_2 & -\xi_1\xi_2^2 \end{bmatrix} \tag{88b}$$

$$\boldsymbol{\Psi}^{\tilde{\lambda}} = \begin{bmatrix} \delta(\boldsymbol{\xi}-\boldsymbol{\xi}_1) & \delta(\boldsymbol{\xi}-\boldsymbol{\xi}_2) & \delta(\boldsymbol{\xi}-\boldsymbol{\xi}_3) \\ \delta(\boldsymbol{\xi}-\boldsymbol{\xi}_1) & \delta(\boldsymbol{\xi}-\boldsymbol{\xi}_2) & \delta(\boldsymbol{\xi}-\boldsymbol{\xi}_3) \cdots \end{bmatrix} \\ \begin{matrix} -\frac{\sqrt{2}}{2}\delta(\boldsymbol{\xi}-\boldsymbol{\xi}_4) & -\frac{\sqrt{2}}{2}\delta(\boldsymbol{\xi}-\boldsymbol{\xi}_5) & -\frac{\sqrt{2}}{2}\delta(\boldsymbol{\xi}-\boldsymbol{\xi}_6) \\ \cdots \frac{\sqrt{2}}{2}\delta(\boldsymbol{\xi}-\boldsymbol{\xi}_4) & \frac{\sqrt{2}}{2}\delta(\boldsymbol{\xi}-\boldsymbol{\xi}_5) & \frac{\sqrt{2}}{2}\delta(\boldsymbol{\xi}-\boldsymbol{\xi}_6) \cdots \end{matrix} \\ \begin{matrix} \delta(\boldsymbol{\xi}-\boldsymbol{\xi}_7) & \delta(\boldsymbol{\xi}-\boldsymbol{\xi}_8) & \delta(\boldsymbol{\xi}-\boldsymbol{\xi}_9) & 1 & \xi_1 & \xi_2 \\ \cdots \delta(\boldsymbol{\xi}-\boldsymbol{\xi}_7) & \delta(\boldsymbol{\xi}-\boldsymbol{\xi}_8) & \delta(\boldsymbol{\xi}-\boldsymbol{\xi}_9) & 0 & 0 & 0 \cdots \end{matrix} \\ \begin{matrix} 0 & 0 & 0 \\ \cdots 1 & \xi_1 & \xi_2 \end{matrix} \Bigg]. \tag{88c}$$

Approximation functions for MITC9s:

$$\boldsymbol{\Psi}^{u} = \begin{bmatrix} \boldsymbol{\Psi}^{QL9} & \mathbf{O} & \mathbf{O} \\ \mathbf{O} & \boldsymbol{\Psi}^{QL9} & \mathbf{O} \\ \mathbf{O} & \mathbf{O} & \boldsymbol{\Psi}^{QL9} \end{bmatrix} \tag{90a}$$

$$\begin{aligned} \boldsymbol{\Phi}^{\tilde{\gamma}_1} = \Bigg[& \frac{1}{4}\left(\sqrt{3}\xi_1 - 1\right)\left(\sqrt{5} - 5\xi_2\right)\xi_2 \ldots \\ & \ldots \frac{1}{2}\left(\sqrt{3}\xi_1 - 1\right)\left(5\xi_2^2 - 1\right) \ldots \\ & \ldots - \frac{1}{4}\left(\sqrt{3}\xi_1 - 1\right)\xi_2\left(5\xi_2 + \sqrt{5}\right) \ldots \\ & \ldots - \frac{1}{4}\left(\sqrt{3}\xi_1 + 1\right)\left(\sqrt{5} - 5\xi_2\right)\xi_2 \ldots \\ & \ldots, \frac{1}{2}\left(\sqrt{3}\xi_1 + 1\right)\left(1 - 5\xi_2^2\right) \ldots \\ & \ldots \frac{1}{4}\left(\sqrt{3}\xi_1 + 1\right)\xi_2\left(5\xi_2 + \sqrt{5}\right)\Bigg] \end{aligned} \tag{90b}$$

$$\boldsymbol{\Phi}^{\tilde{\lambda}_1} = \begin{bmatrix} \delta(\boldsymbol{\xi}-\boldsymbol{\xi}_1) & \delta(\boldsymbol{\xi}-\boldsymbol{\xi}_2) & \delta(\boldsymbol{\xi}-\boldsymbol{\xi}_3) & \delta(\boldsymbol{\xi}-\boldsymbol{\xi}_4) \ldots \\ \ldots \delta(\boldsymbol{\xi}-\boldsymbol{\xi}_5) & \delta(\boldsymbol{\xi}-\boldsymbol{\xi}_6) \end{bmatrix}. \tag{90c}$$

Approximation functions for MITC4:

$$\boldsymbol{\Psi}^{u} = \begin{bmatrix} \boldsymbol{\Psi}^{QL4} & \mathbf{O} & \mathbf{O} \\ \mathbf{O} & \boldsymbol{\Psi}^{QL4} & \mathbf{O} \\ \mathbf{O} & \mathbf{O} & \boldsymbol{\Psi}^{QL4} \end{bmatrix} \tag{89a}$$

$$\boldsymbol{\Phi}^{\tilde{\gamma}_1} = \begin{bmatrix} \frac{1}{2}(\xi_2 - 1) & \frac{1}{2}(\xi_2 + 1) \end{bmatrix} \tag{89b}$$

$$\boldsymbol{\Phi}^{\tilde{\lambda}_1} = \begin{bmatrix} \delta(\boldsymbol{\xi}-\boldsymbol{\xi}_1) & \delta(\boldsymbol{\xi}-\boldsymbol{\xi}_2) \end{bmatrix}. \tag{89c}$$

Approximation functions for MITC16s:

$$\boldsymbol{\Psi}^{u} = \begin{bmatrix} \boldsymbol{\Psi}^{QL16} & \mathbf{O} & \mathbf{O} \\ \mathbf{O} & \boldsymbol{\Psi}^{QL16} & \mathbf{O} \\ \mathbf{O} & \mathbf{O} & \boldsymbol{\Psi}^{QL16} \end{bmatrix} \tag{91a}$$

A MITC APPROXIMATION FUNCTIONS

$$
\begin{aligned}
\boldsymbol{\Phi}^{\tilde{\gamma}_1} = \Bigg[& \frac{\left(\sqrt{5}-5\xi_1\right)\xi_1(c-\xi_2)(c+\xi_2)(d-\xi_2)}{4\left(d^3-c^2d\right)} \cdots \\
& \cdots \frac{\left(\sqrt{5}-5\xi_1\right)\xi_1(c-\xi_2)(d-\xi_2)(d+\xi_2)}{4c(c-d)(c+d)} \cdots \\
& \cdots \frac{\left(\sqrt{5}-5\xi_1\right)\xi_1(c+\xi_2)(d-\xi_2)(d+\xi_2)}{4c(c-d)(c+d)} \cdots \\
& \cdots \frac{\left(\sqrt{5}-5\xi_1\right)\xi_1(c-\xi_2)(c+\xi_2)(d+\xi_2)}{4\left(d^3-c^2d\right)} \cdots \\
& \cdots \frac{\left(1-5\xi_1^2\right)\left(\xi_2^2-c^2\right)(d-\xi_2)}{2\left(d^3-c^2d\right)} \cdots \\
& \cdots \frac{\left(1-5\xi_1^2\right)(c-\xi_2)\left(\xi_2^2-d^2\right)}{2\left(c^3-cd^2\right)} \cdots \\
& \cdots \frac{\left(1-5\xi_1^2\right)(c+\xi_2)\left(\xi_2^2-d^2\right)}{2\left(c^3-cd^2\right)} \cdots \\
& \cdots \frac{\left(1-5\xi_1^2\right)\left(\xi_2^2-c^2\right)(d+\xi_2)}{2\left(d^3-c^2d\right)} \cdots \\
& \cdots \frac{\xi_1\left(5\xi_1+\sqrt{5}\right)(c-\xi_2)(c+\xi_2)(d-\xi_2)}{4d(c-d)(c+d)} \cdots \\
& \cdots \frac{\xi_1\left(5\xi_1+\sqrt{5}\right)(c-\xi_2)\left(\xi_2^2-d^2\right)}{4\left(c^3-cd^2\right)} \cdots \\
& \cdots \frac{\xi_1\left(5\xi_1+\sqrt{5}\right)(c+\xi_2)\left(\xi_2^2-d^2\right)}{4\left(c^3-cd^2\right)} \cdots \\
& \cdots \frac{\xi_1\left(5\xi_1+\sqrt{5}\right)(c-\xi_2)(c+\xi_2)(d+\xi_2)}{4d(c-d)(c+d)} \Bigg]
\end{aligned}
\tag{91b}
$$

$$
\begin{aligned}
\boldsymbol{\Phi}^{\underline{\lambda}_1} = & \left[\delta\left(\boldsymbol{\xi}-\boldsymbol{\xi}_1\right) \quad \delta\left(\boldsymbol{\xi}-\boldsymbol{\xi}_2\right) \quad \delta\left(\boldsymbol{\xi}-\boldsymbol{\xi}_3\right) \quad \delta\left(\boldsymbol{\xi}-\boldsymbol{\xi}_4\right) \ldots\right. \\
& \ldots \delta\left(\boldsymbol{\xi}-\boldsymbol{\xi}_5\right) \quad \delta\left(\boldsymbol{\xi}-\boldsymbol{\xi}_6\right) \quad \delta\left(\boldsymbol{\xi}-\boldsymbol{\xi}_7\right) \ldots \\
& \ldots \delta\left(\boldsymbol{\xi}-\boldsymbol{\xi}_8\right) \quad \delta\left(\boldsymbol{\xi}-\boldsymbol{\xi}_9\right) \quad \delta\left(\boldsymbol{\xi}-\boldsymbol{\xi}_{10}\right) \ldots \\
& \left. \ldots \delta\left(\boldsymbol{\xi}-\boldsymbol{\xi}_{11}\right) \quad \delta\left(\boldsymbol{\xi}-\boldsymbol{\xi}_{12}\right)\right] .
\end{aligned}
\tag{91c}
$$

In Figures 11, 12, 13, 12, 15, 16, 17 are represented the MITC elements studied in this work and its characteristics, including degrees of freedom at each node and *tying points* location.

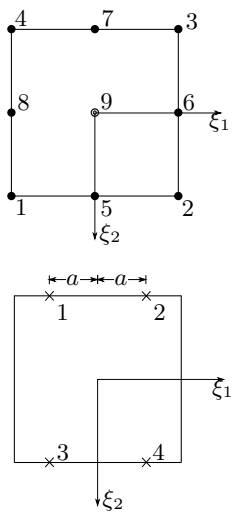

- nodes for w and θ_α interpolation
- nodes for θ_α interpolation

$\boldsymbol{\Psi}^w \in E^{QS8}$, $E^{QS8} = \{1, \xi_1, \xi_2, \xi_1^2, \xi_1\xi_2, \xi_2^2, \xi_1^2\xi_2, \xi_1\xi_2^2\}$

$\boldsymbol{\Psi}^\theta \in E^{QL9}$, $E^{QL9} = \{1, \xi_1, \xi_2, \xi_1^2, \xi_1\xi_2, \xi_2^2, \xi_1^2\xi_2, \xi_1\xi_2^2, \xi_1^2\xi_2^2\}$

× *tying points*

$a = \frac{\sqrt{3}}{3}$

Figure 11: Degrees of freedom associated to each node, *tying points* in ξ_1 direction, for MITC9p.

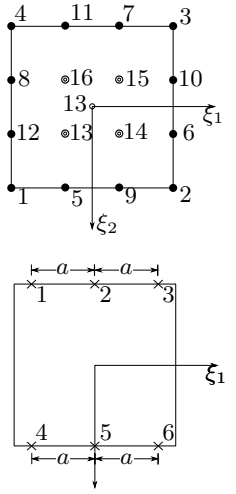

- nodes for w and θ_α interpolation
- nodes for θ_α interpolation
- nodes for w interpolation

$\boldsymbol{\Psi}^w \in E^{QL16} \cap E^{T15}$, $\boldsymbol{\Psi}^w \in \{1, \xi_1, \xi_2, \xi_1^2, \xi_1\xi_2, \xi_2^2, \xi_1^3, \xi_1^2\xi_2, \xi_1\xi_2^2, \xi_2^3, \xi_2\xi_1^3, \xi_1^2\xi_2^2, \xi_1\xi_2^3, \xi_1^3\xi_2^2\}$

$\boldsymbol{\Psi}^\theta \in E^{QL16}$, $E^{QL16} = \{1, \xi_1, \xi_2, \xi_1^2, \xi_1\xi_2, \xi_2^2, \xi_1^3, \xi_1^2\xi_2, \xi_1\xi_2^2, \xi_2^3, \xi_2\xi_1^3, \xi_1^2\xi_2^2, \xi_1\xi_2^3, \xi_1^3\xi_2^2, \xi_1^2\xi_2^3, \xi_1^3\xi_2^3\}$

× *tying points*

$a = \sqrt{\frac{3}{5}}$

Figure 12: Degrees of freedom associated to each node, *tying points* in ξ_1 direction, for MITC16p.

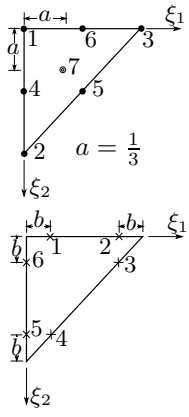

- nodes for w and θ_α interpolation
- nodes for θ_α interpolation

$\boldsymbol{\Psi}^w \in E^{T6}$, $E^{T6} = \{1, \xi_1, \xi_2, \xi_1^2, \xi_1\xi_2, \xi_2^2\}$

$\boldsymbol{\Psi}^\theta = \{1, \xi_1, \xi_2, \xi_1^2, \xi_1\xi_2, \xi_2^2, \xi_1\xi_2\,(1-\xi_1-\xi_2)\}$

× *tying points*

$b = \frac{1}{2} - \frac{\sqrt{3}}{6}$

Figure 13: Degrees of freedom associated to each node, *tying points* in ξ_1 direction, for MITC7p.

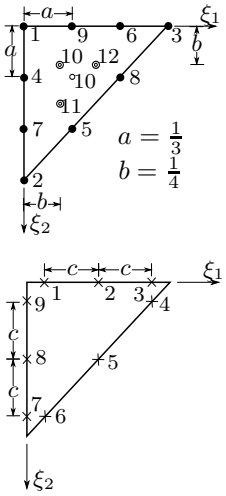

- nodes for w and θ_α interpolation
- nodes for θ_α interpolation
- nodes for w interpolation

$\mathbf{\Psi}^w \in E^{T10}$, $E^{T10} = \{1, \xi_1, \xi_2, \xi_1^2, \xi_1\xi_2, \xi_2^2, \xi_1^3, \xi_1^2\xi_2, \xi_1\xi_2^2, \xi_2^3\}$

$\mathbf{\Psi}^\theta = \{1, \xi_1, \xi_2, \xi_1^2, \xi_2\xi_1, \xi_2^2, \xi_1^3, \xi_2\xi_1^2, \xi_2^2\xi_1, \xi_2^3, \xi_2\xi_1^2(\xi_2+\xi_1), \xi_2^2\xi_1(\xi_2+\xi_1)\}$

× *tying points*

$c = \sqrt{\frac{3}{20}}$

Figure 14: Degrees of freedom associated to each node, *tying points* in ξ_1 direction, for MITC12p.

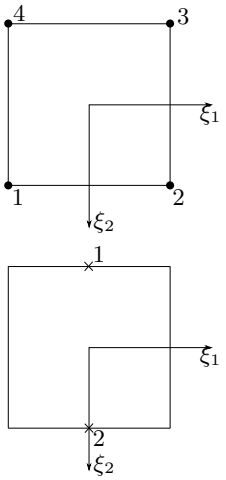

- nodes for w and θ_α interpolation

$\mathbf{\Psi}^w, \mathbf{\Psi}^\theta \in E^{QL4}$,

$E^{QL4} = \{1, \xi_1, \xi_2, \xi_1\xi_2\}$

× *tying points*

Figure 15: Degrees of freedom associated to each node, *tying points* in ξ_1 direction, for MITC4.

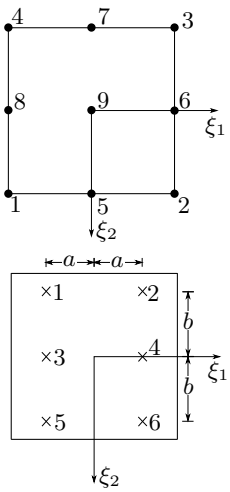

- nodes for w and θ_α interpolation

$\mathbf{\Psi}^w, \mathbf{\Psi}^\theta \in E^{QL9}$, $E^{QL9} = \{1, \xi_1, \xi_2, \xi_1^2, \xi_1\xi_2, \xi_2^2, \xi_1^2\xi_2, \xi_1\xi_2^2, \xi_1^2\xi_2^2\}$

× *tying points*

$a = \frac{\sqrt{3}}{3}$

$b = \sqrt{\frac{3}{5}}$

Figure 16: Degrees of freedom associated to each node, *tying points* in ξ_1 direction, for MITC9s.

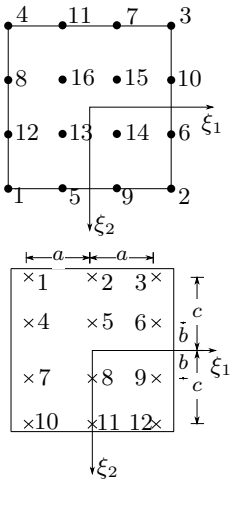

- nodes for w and θ_α interpolation

$\mathbf{\Psi}^w, \mathbf{\Psi}^\theta \in E^{QL16}$, $E^{QL16} = \{1, \xi_1, \xi_2, \xi_1^2, \xi_1\xi_2, \xi_2^2, \xi_1^3, \xi_1^2\xi_2, \xi_1\xi_2^2, \xi_2^3, \xi_1^3\xi_2, \xi_1^2\xi_2^2, \xi_1\xi_2^3, \xi_1^3\xi_2^3\}$

× *tying points*

$a = \sqrt{\frac{3}{5}}$

$b = \sqrt{\frac{30-\sqrt{480}}{70}}$

$c = \sqrt{\frac{30+\sqrt{480}}{70}}$

Figure 17: Degrees of freedom associated to each node, *tying points* in ξ_1 direction, for MITC16s.

References

Bathe, K.-J. (1996). *Finite Element Procedures*. Prentice Hall.

Dvorkin, E. N. and K.-J. Bathe (1984). A continuum mechanics based four-node shell element for general nonlinear analysis. *Engineering Computations*, *1*(1), 77–88.

Hinton, E. and H. C. Huang (1986). A family of quadrilateral Mindlin plate elements with substitute shear strain fields. *Computers & Structures*, *23*(3), 409–431.